Supporting Information

Fluorescence Tuning of Zn(II)-Based Metallo-supramolecular Coordination Polymers and Their Application for Picric Acid Detection

*Hong-Qing Li, Zhong-Yu Ding, Yao Pan, Chun-Hua Liu and Yuan-Yuan Zhu**

School of Chemistry and Chemical Engineering, Hefei University of Technology and Anhui Key Laboratory of Advanced Functional Materials and Devices, Hefei 230009, China

yyzhu@hfut.edu.cn

List of Supporting Information

SI1 ^{1}H NMR and ^{13}C NMR spectra

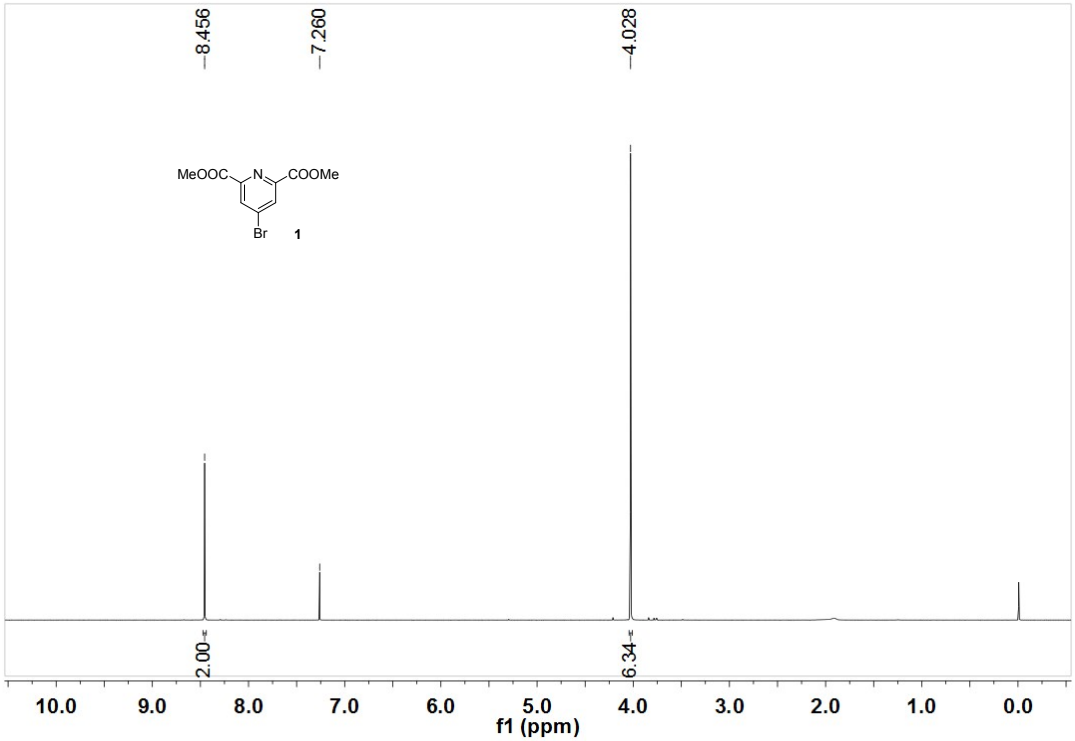

Figure S1. ^{1}H NMR spectrum of compound **1** (400 MHz) in $CDCl_3$ (10 mM).

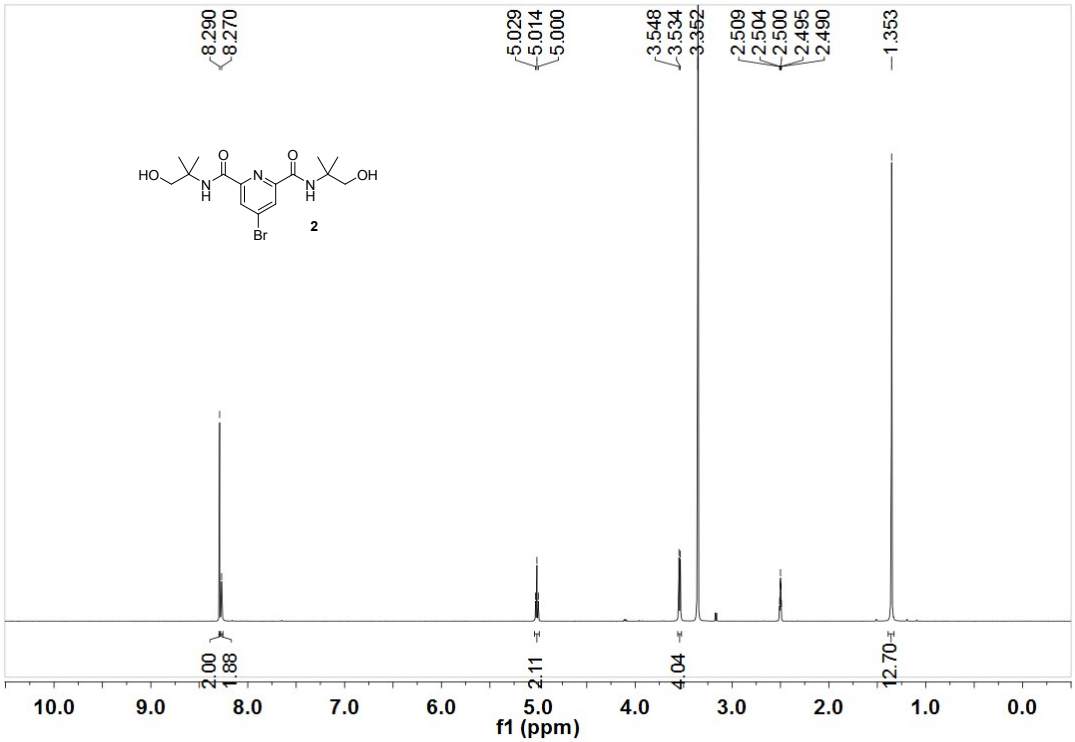

Figure S2. ^{1}H NMR spectrum of compound **2** (400 MHz) in DMSO-d_6 (10 mM).

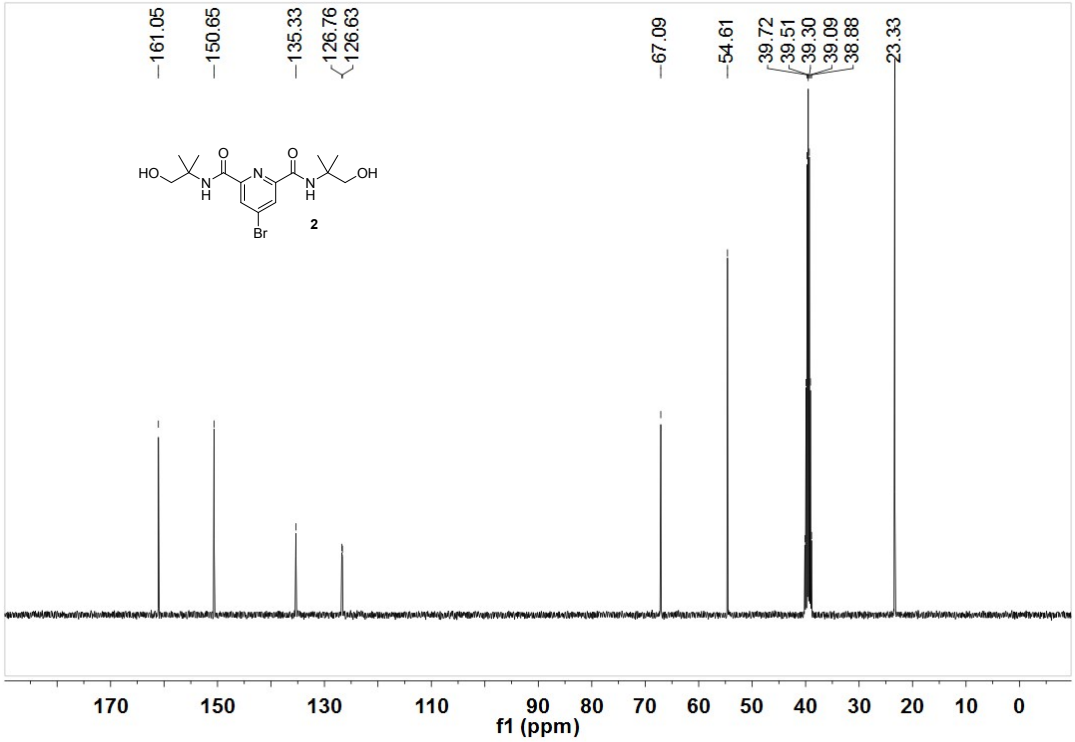

Figure S3. ^{13}C NMR spectrum of compound **2** (100 MHz) in DMSO-d_6 (50 mM).

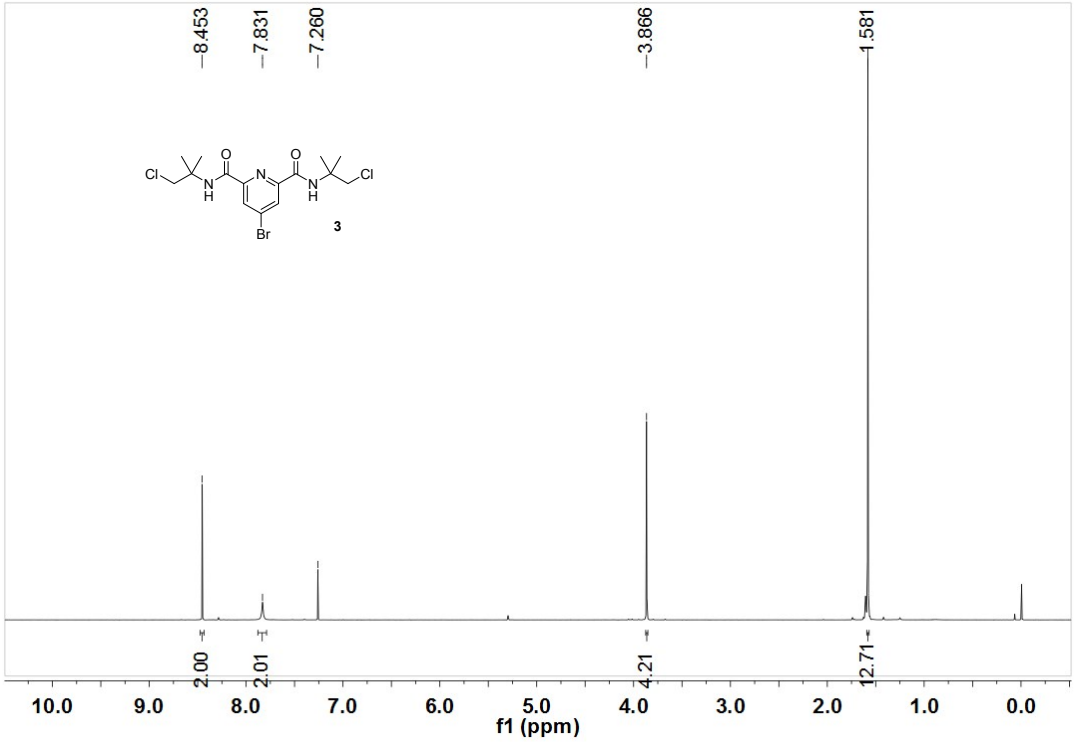

Figure S4. ^{1}H NMR spectrum of compound **3** (400 MHz) in $CDCl_3$ (10 mM).

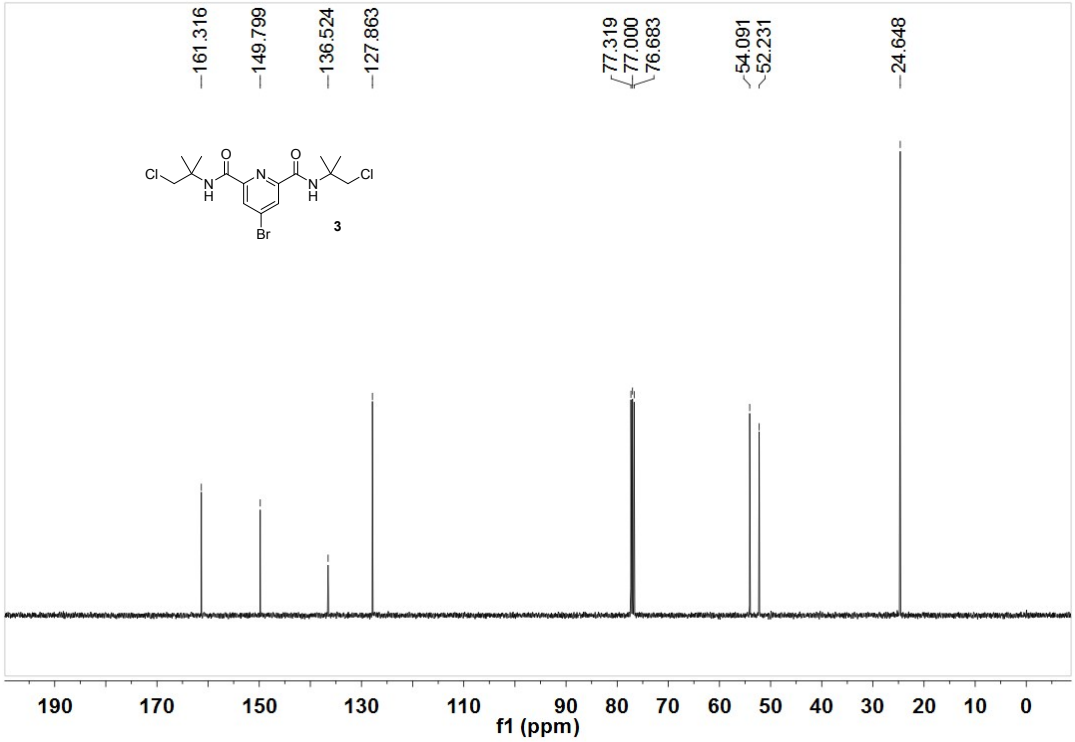

Figure S5. ^{13}C NMR spectrum of compound **3** (100 MHz) in $CDCl_3$ (50 mM).

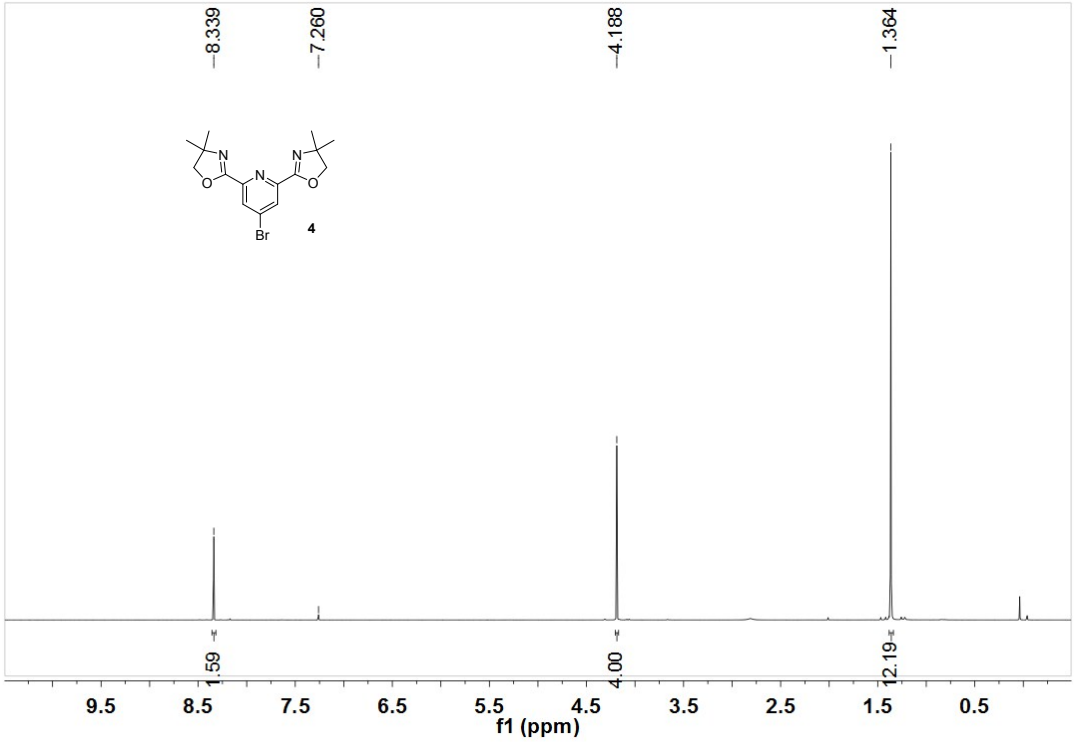

Figure S6. ^{1}H NMR spectrum of compound **4** (600 MHz) in $CDCl_3$ (30 mM).

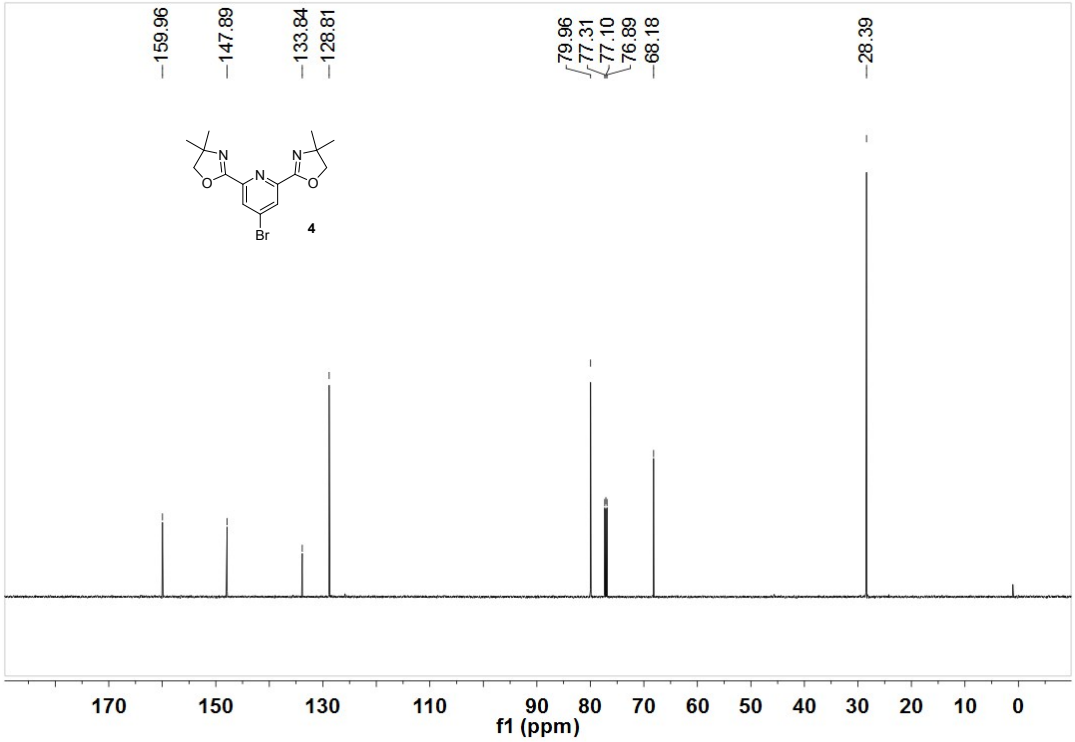

Figure S7. ^{13}C NMR spectrum of compound **4** (125 MHz) in $CDCl_3$ (50 mM).

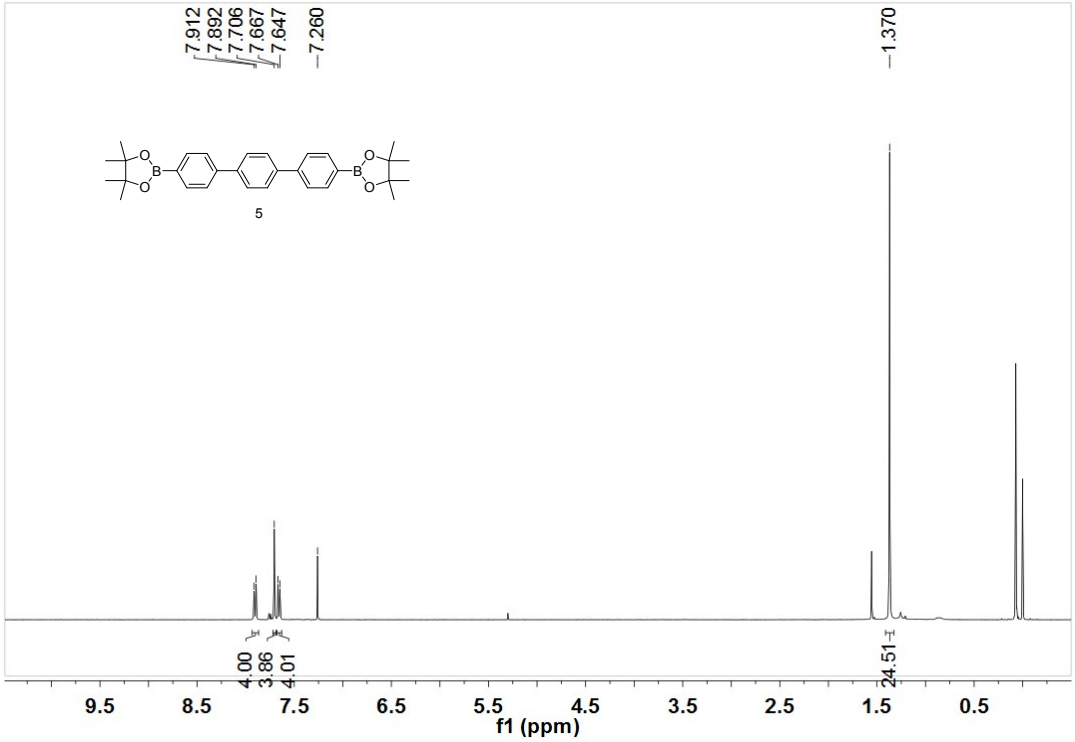

Figure S8. ^{1}H NMR spectrum of compound **5** (400 MHz) in $CDCl_3$ (10 mM).

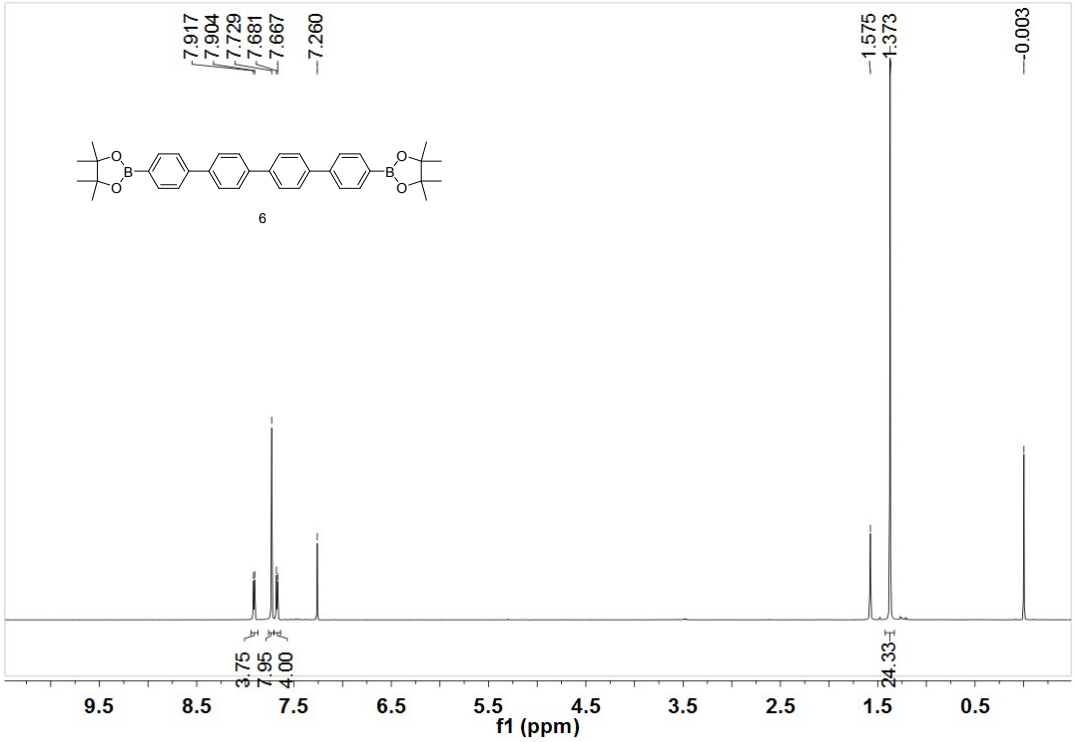

Figure S9. ^{1}H NMR spectrum of compound **6** (400 MHz) in $CDCl_3$ (10 mM).

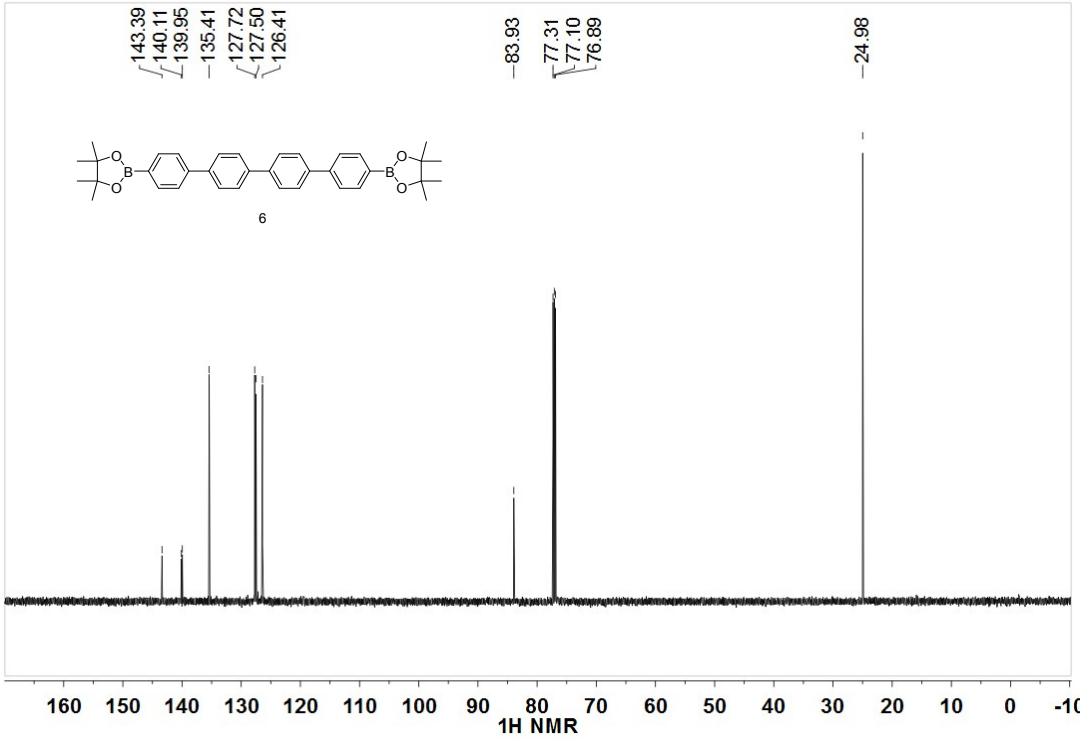

Figure S10. ^{13}C NMR spectrum of compound **6** (125 MHz) in $CDCl_3$ (50 mM).

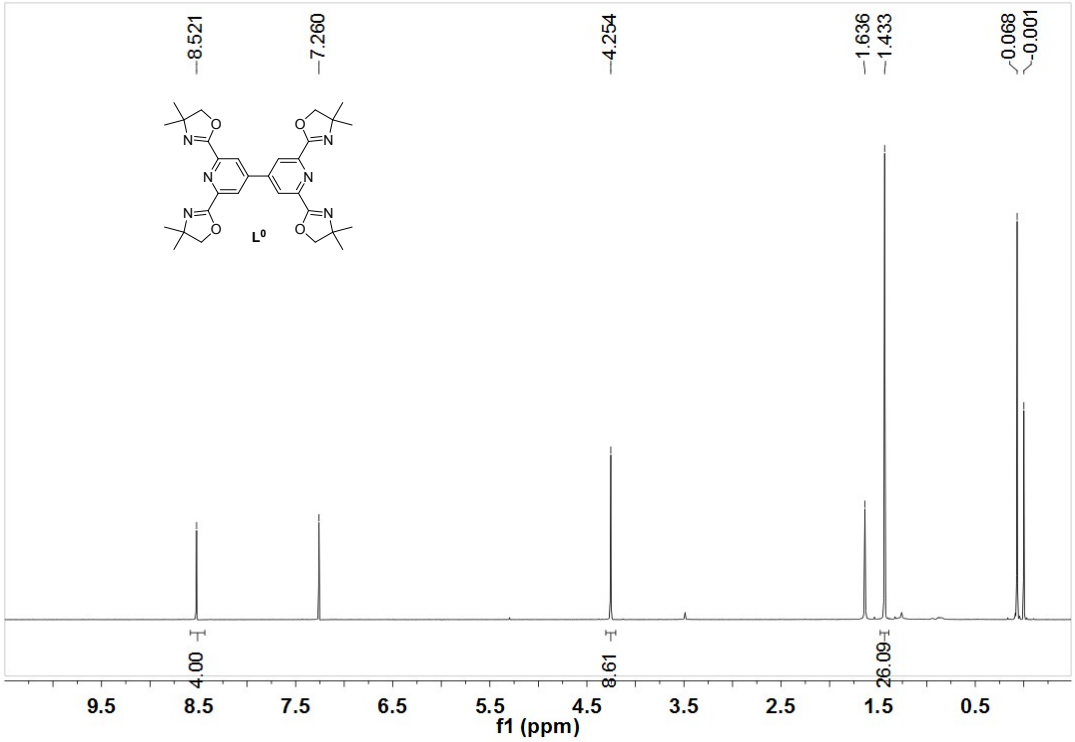

Figure S11. ^{1}H NMR spectrum of compound **L^{0}** (600 MHz) in $CDCl_3$ (10 mM).

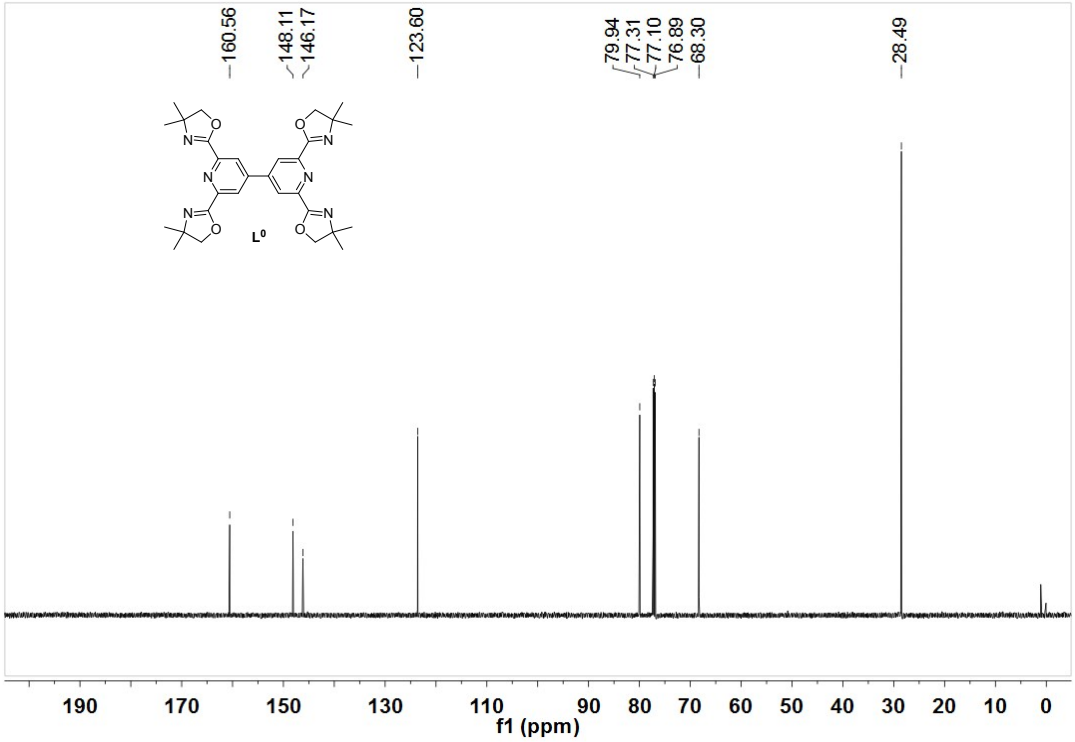

Figure S12. ^{13}C NMR spectrum of compound **L^{0}** (125 MHz) in $CDCl_3$ (50 mM).

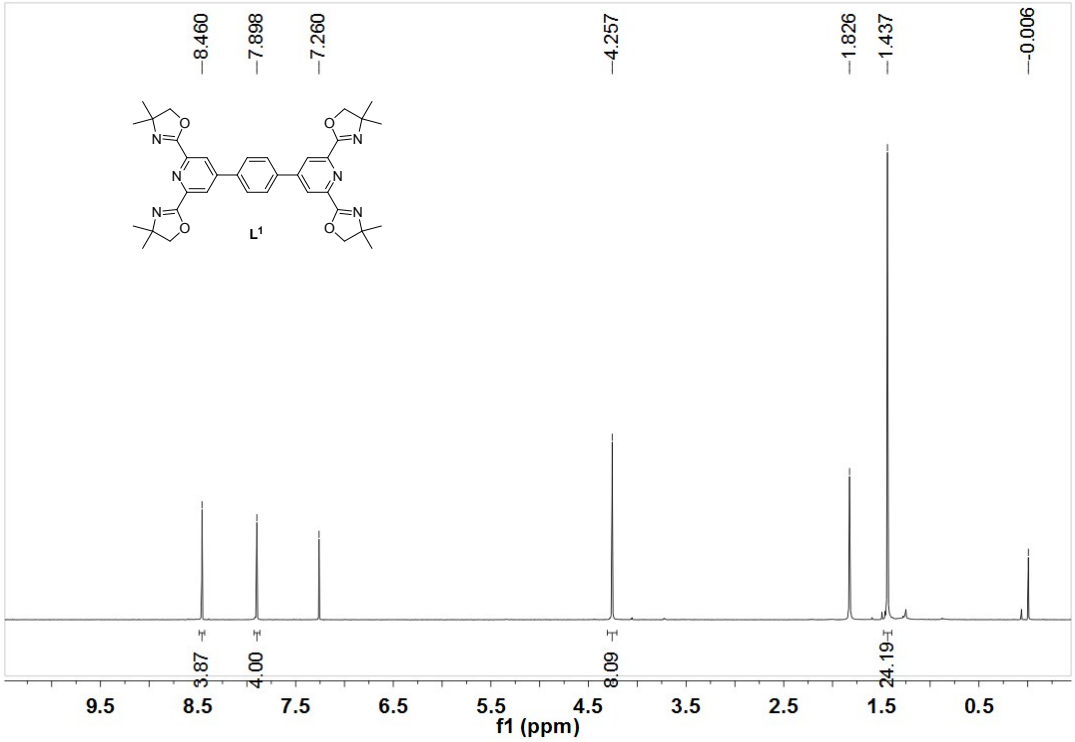

Figure S13. ^{1}H NMR spectrum of compound **L¹** (400 MHz) in $CDCl_3$ (10 mM).

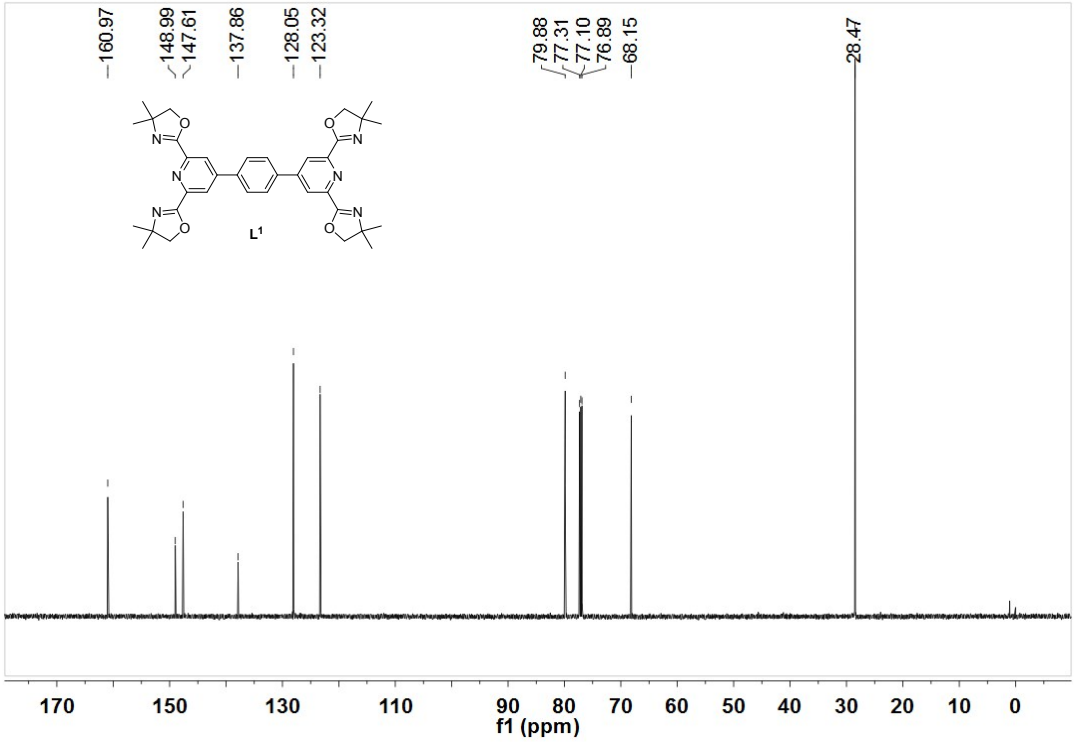

Figure S14. ^{13}C NMR spectrum of compound **L¹** (100 MHz) in $CDCl_3$ (50 mM).

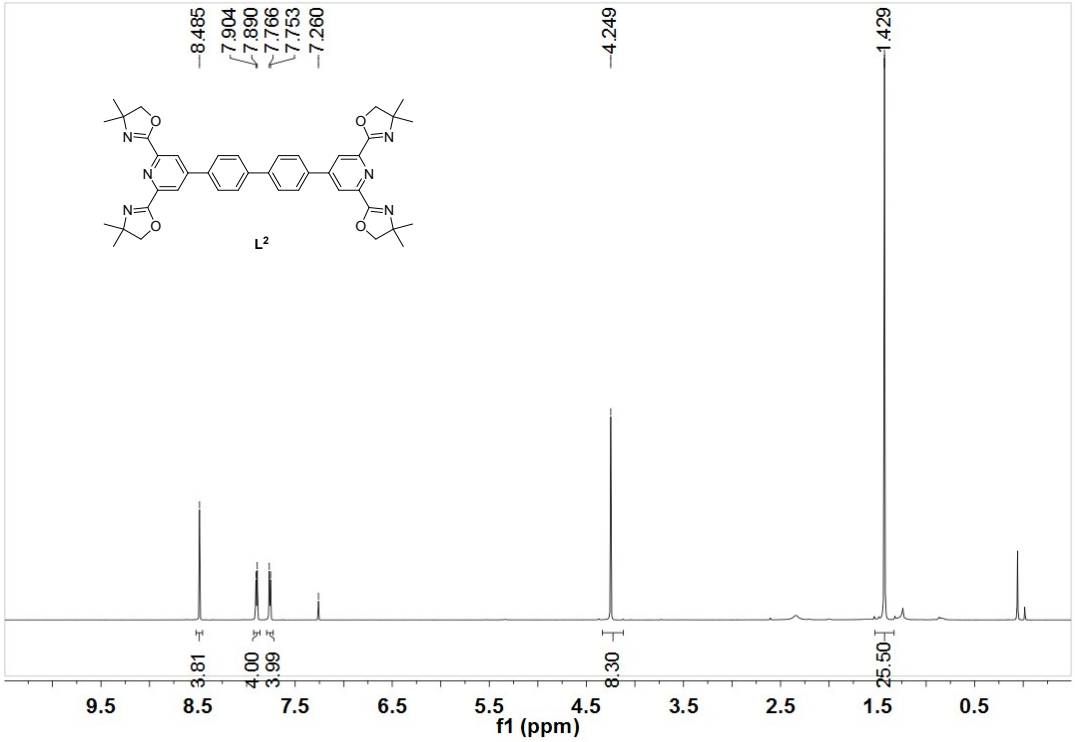

Figure S15. ^{1}H NMR spectrum of compound **L²** (600 MHz) in $CDCl_3$ (10 mM).

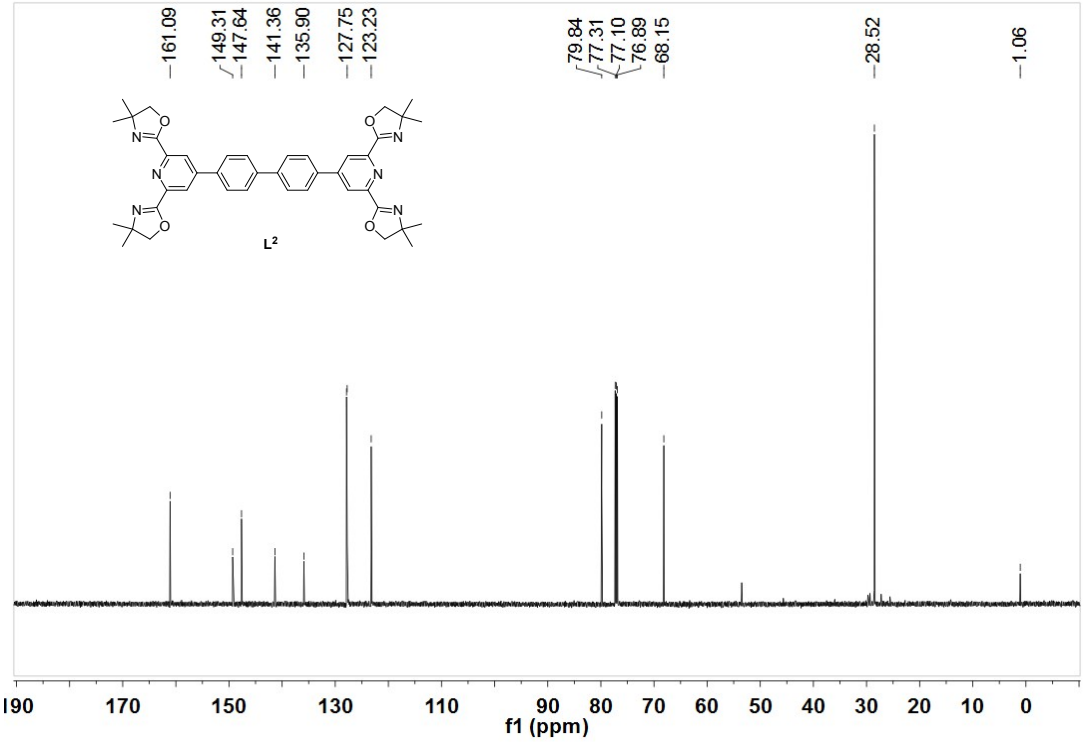

Figure S16. ^{13}C NMR spectrum of compound **L²** (125 MHz) in $CDCl_3$ (40 mM).

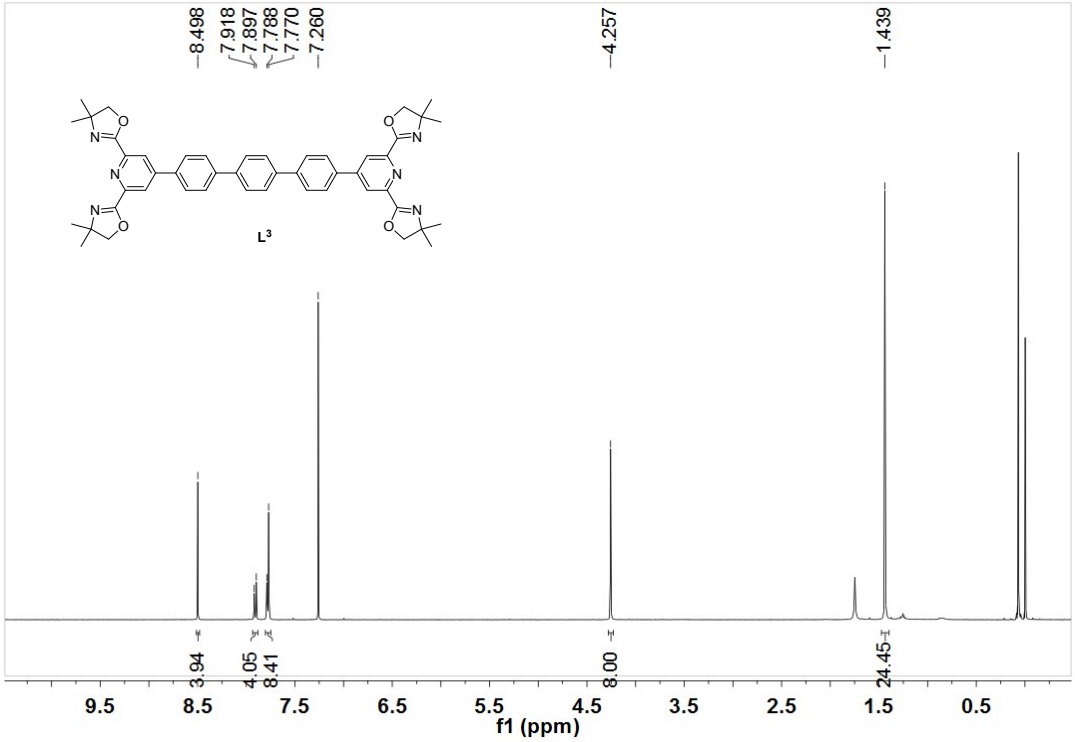

Figure S17. ^{1}H NMR spectrum of compound **L³** (400 MHz) in $CDCl_3$ (10 mM).

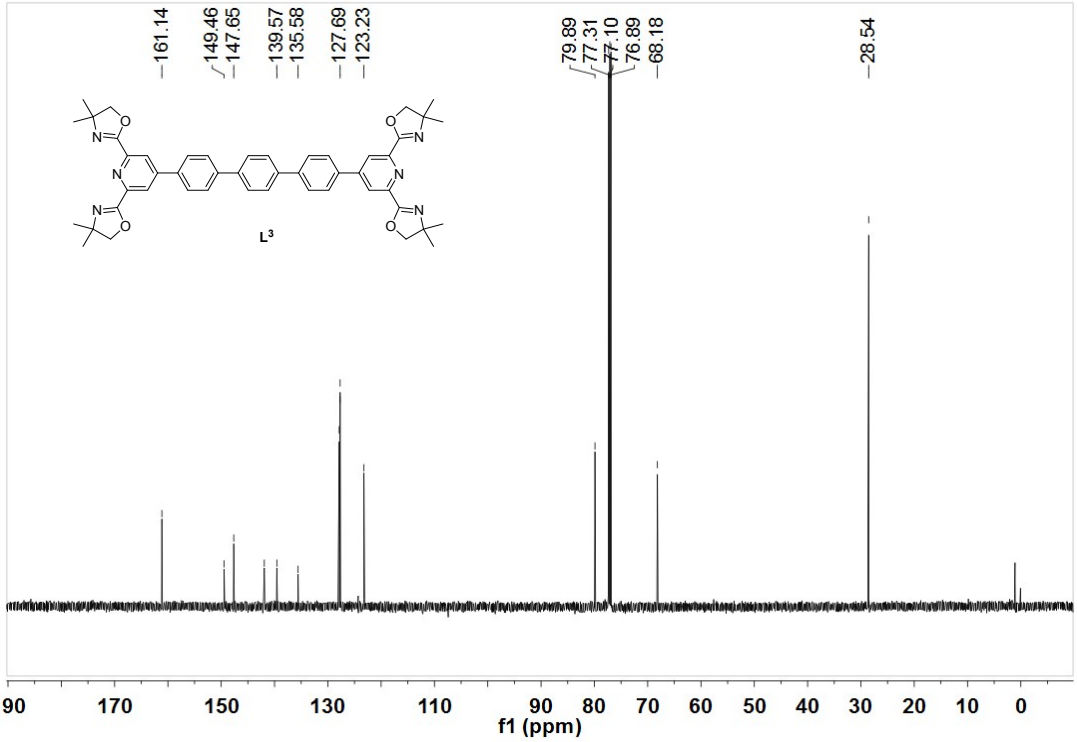

Figure S18. ^{13}C NMR spectrum of compound **L³** (100 MHz) in $CDCl_3$ (50 mM).

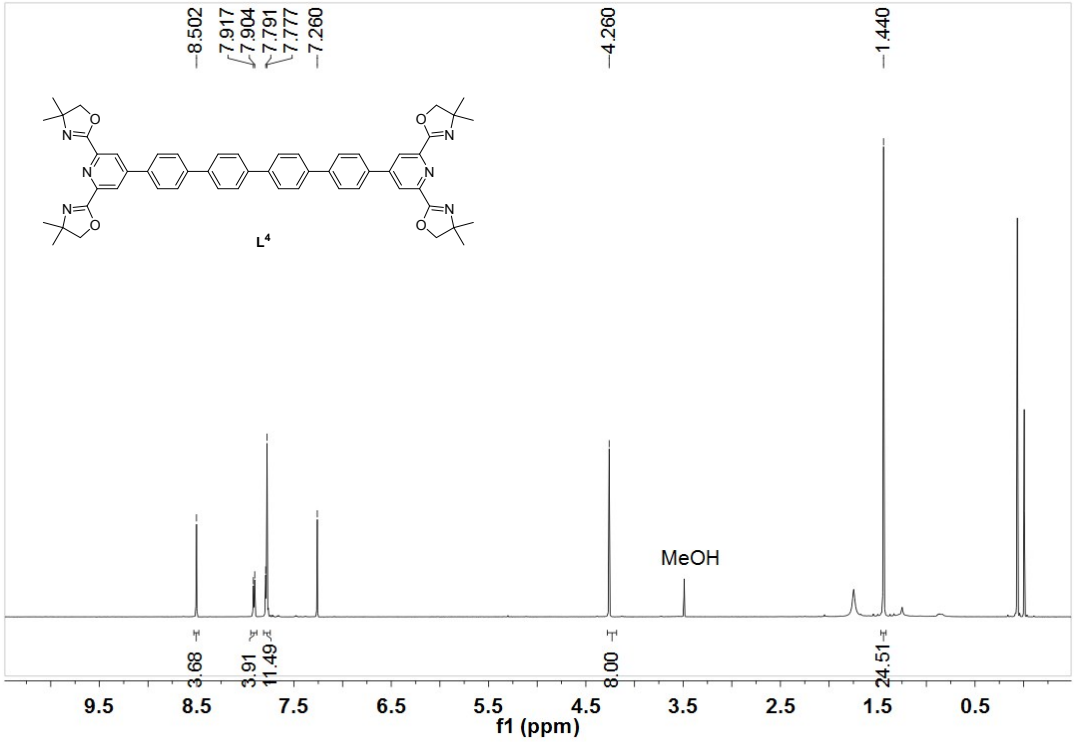

Figure S19. ^{1}H NMR spectrum of compound **L^{4}** (600 MHz) in $CDCl_3$ (10 mM).

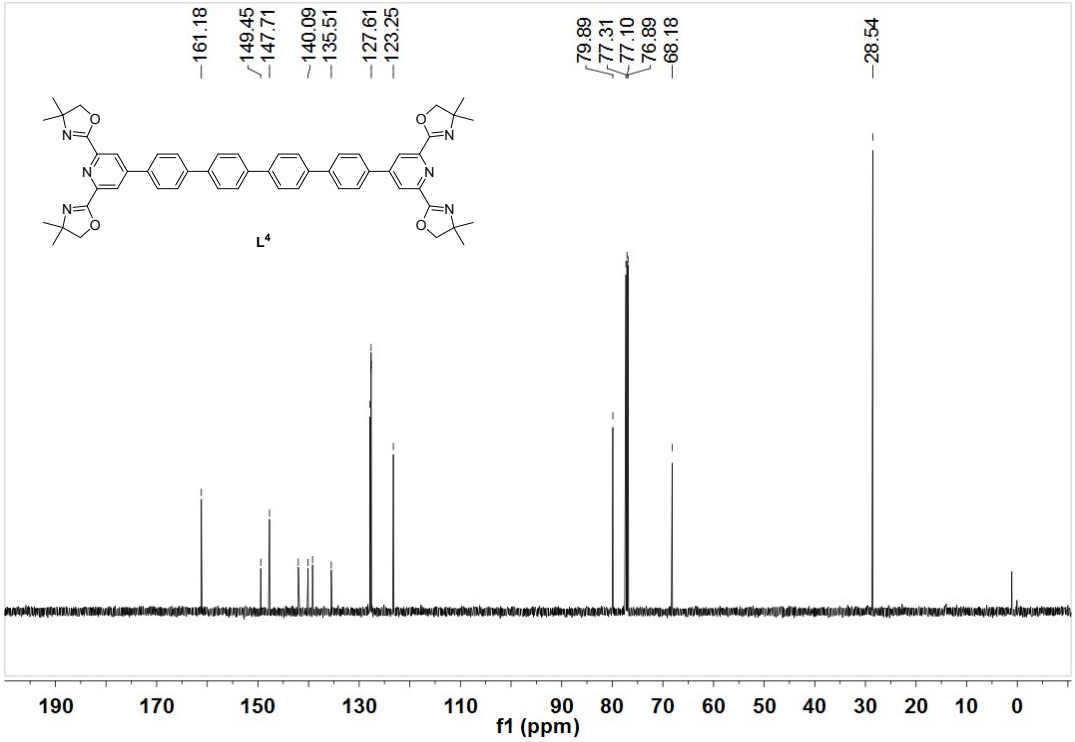

Figure S20. ^{13}C NMR spectrum of compound **L^{4}** (125 MHz) in $CDCl_3$ (50 mM).

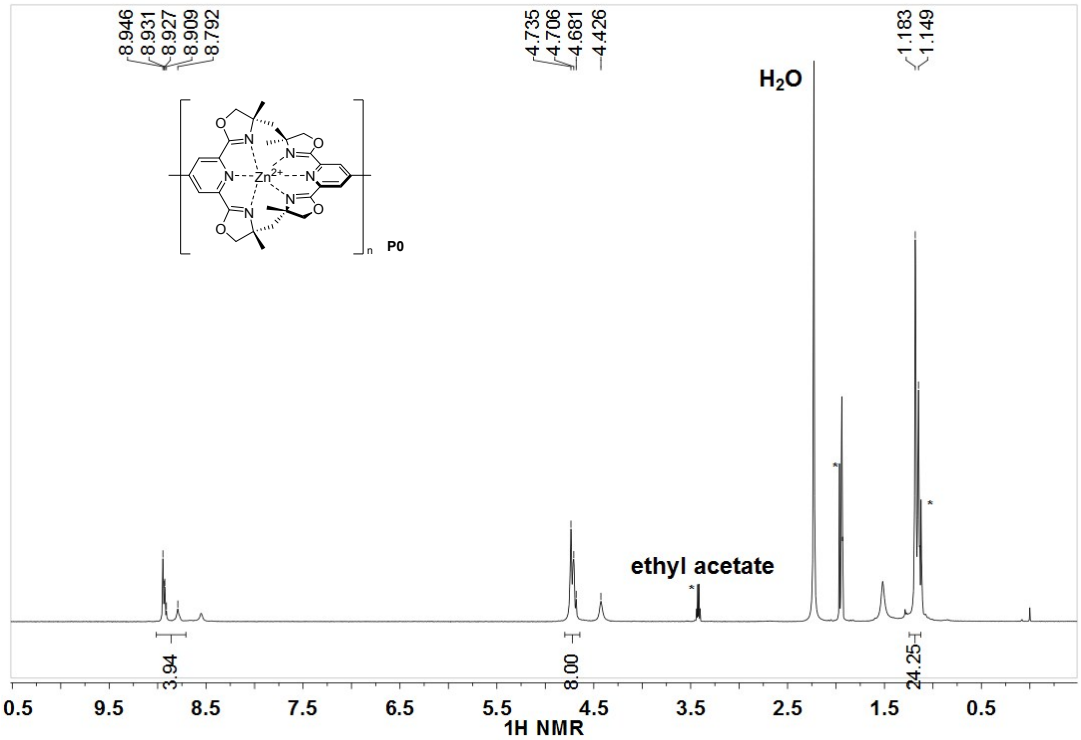

Figure S21. ^{1}H NMR spectrum of **P0** (600 MHz) in CD_3CN (10 mM).

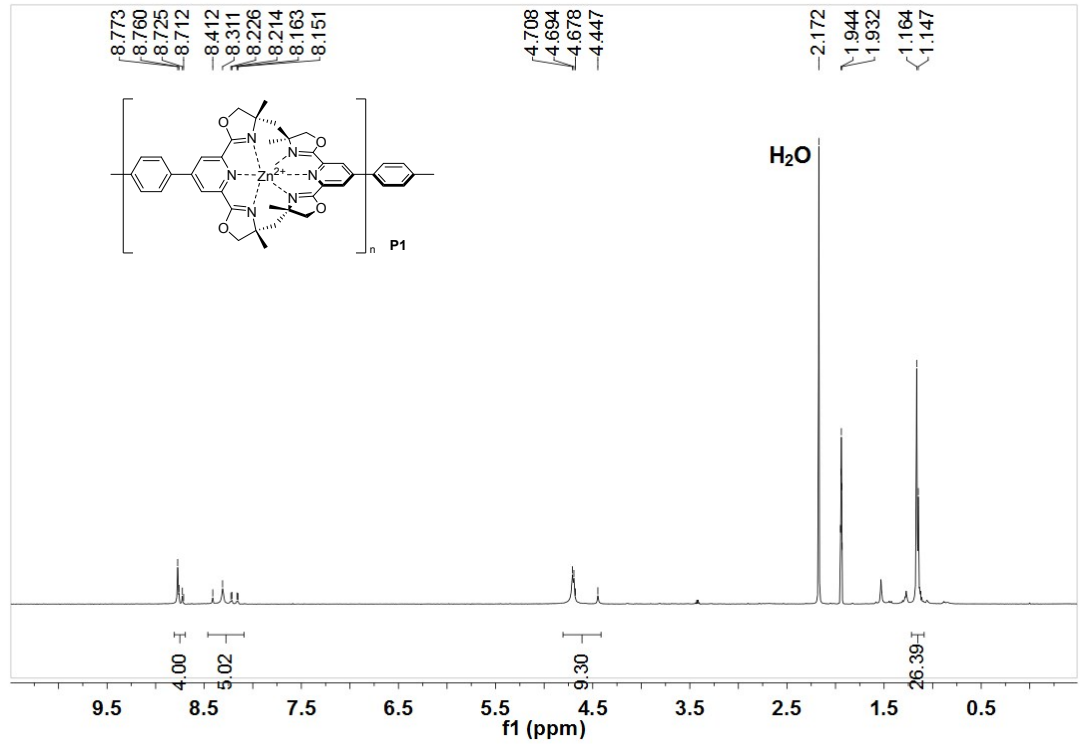

Figure S22. ^{1}H NMR spectrum of **P1** (600 MHz) in CD_3CN (10 mM).

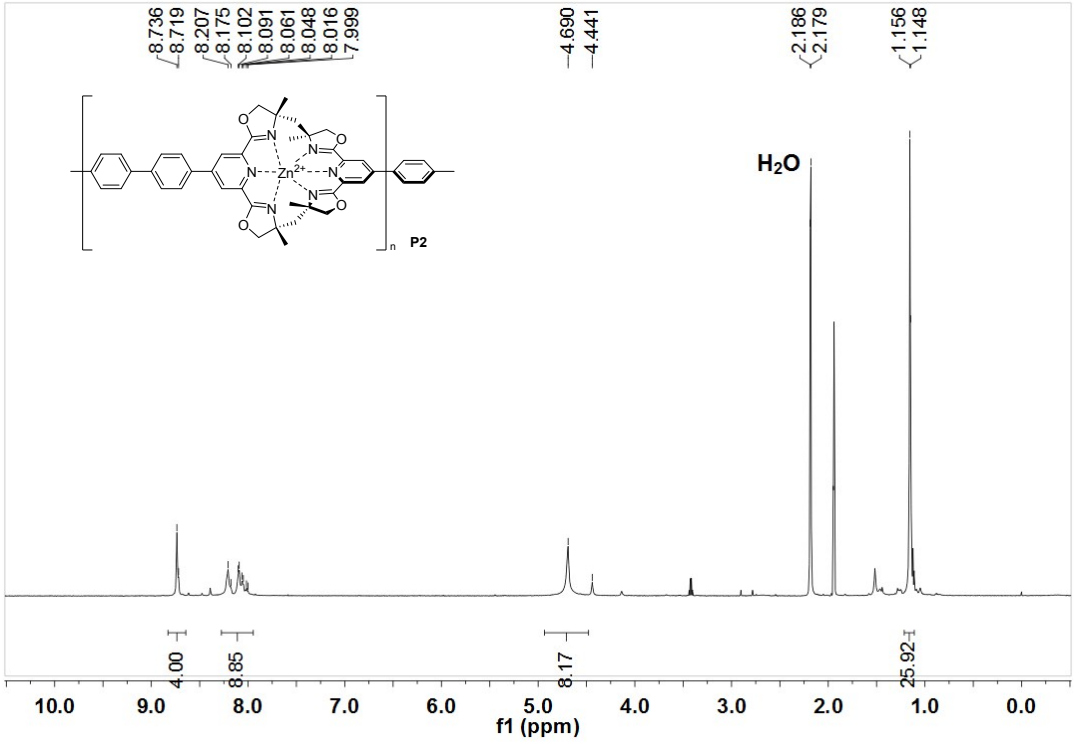

Figure S23. ^{1}H NMR spectrum of **P2** (600 MHz) in CD_3CN (10 mM).

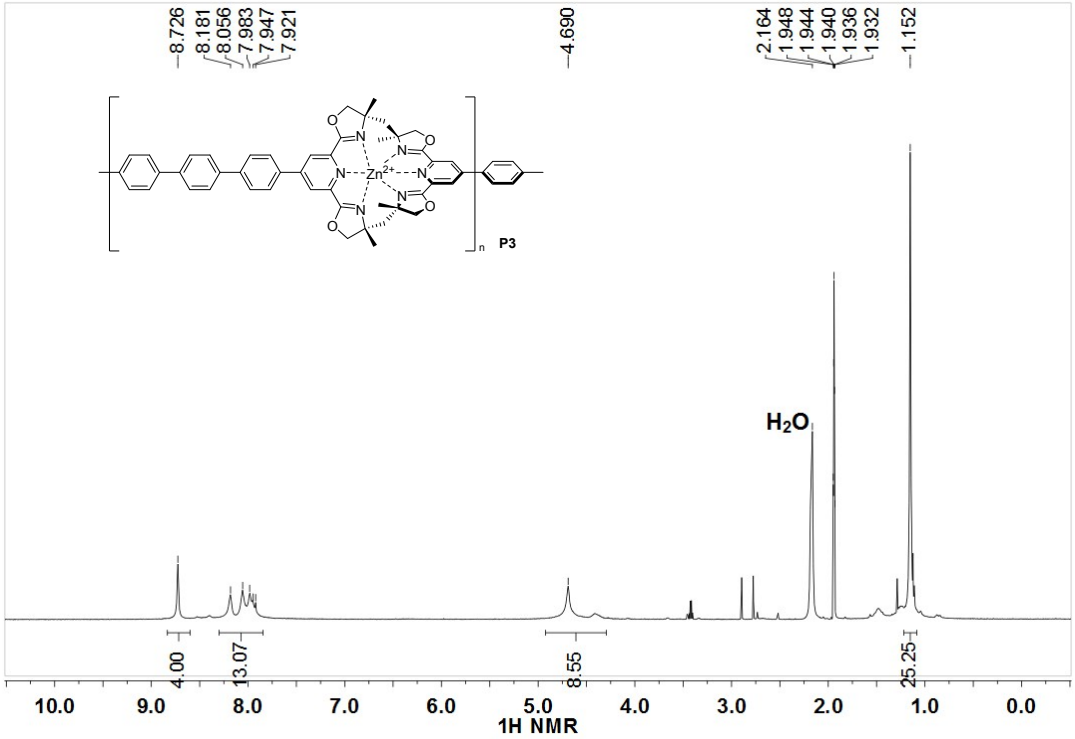

Figure S24. ^{1}H NMR spectrum of **P3** (600 MHz) in CD_3CN (10 mM).

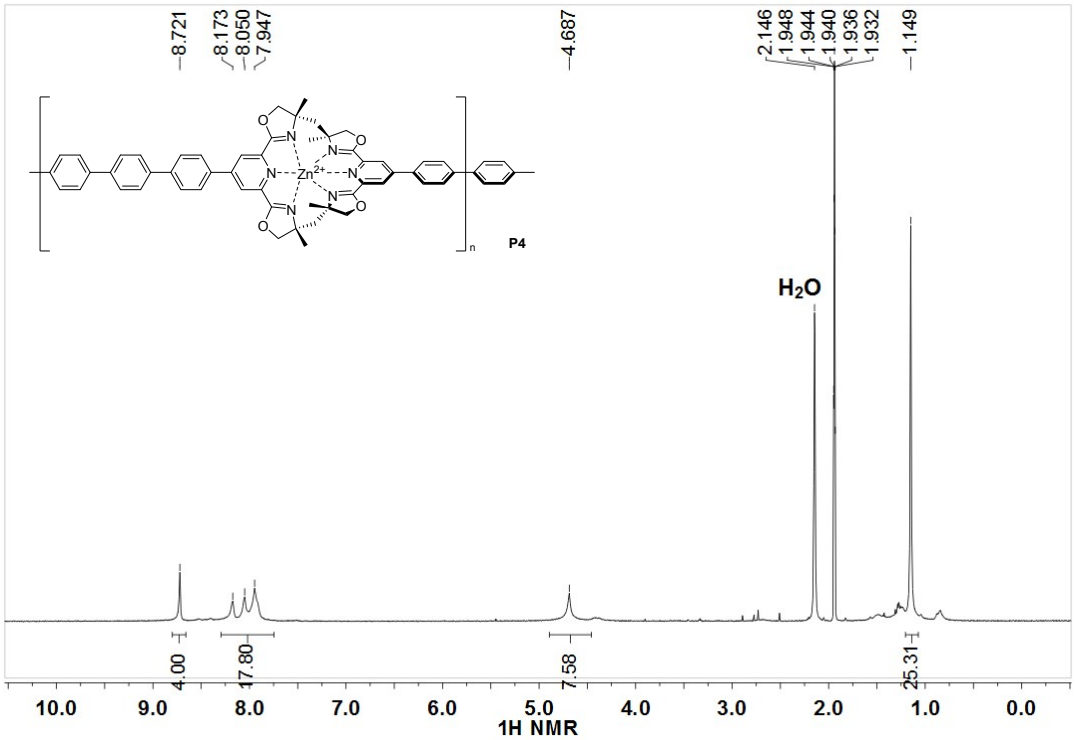

Figure S25. ^{1}H NMR spectrum of **P4** (600 MHz) in CD_3CN (10 mM).

SI2 Structural characterization of coordination polymers.

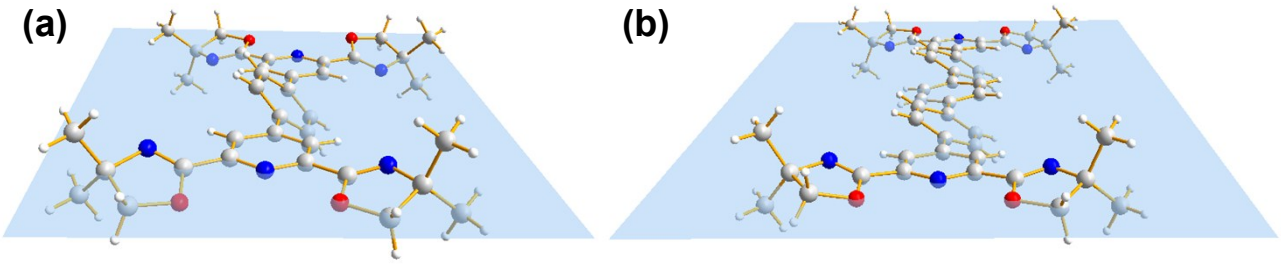

Figure S26. The side view of molecular structures of (a) **L**[1] and (b) **L**[3], revealing that two pybox planes are almost parallel with each other in two ligands.

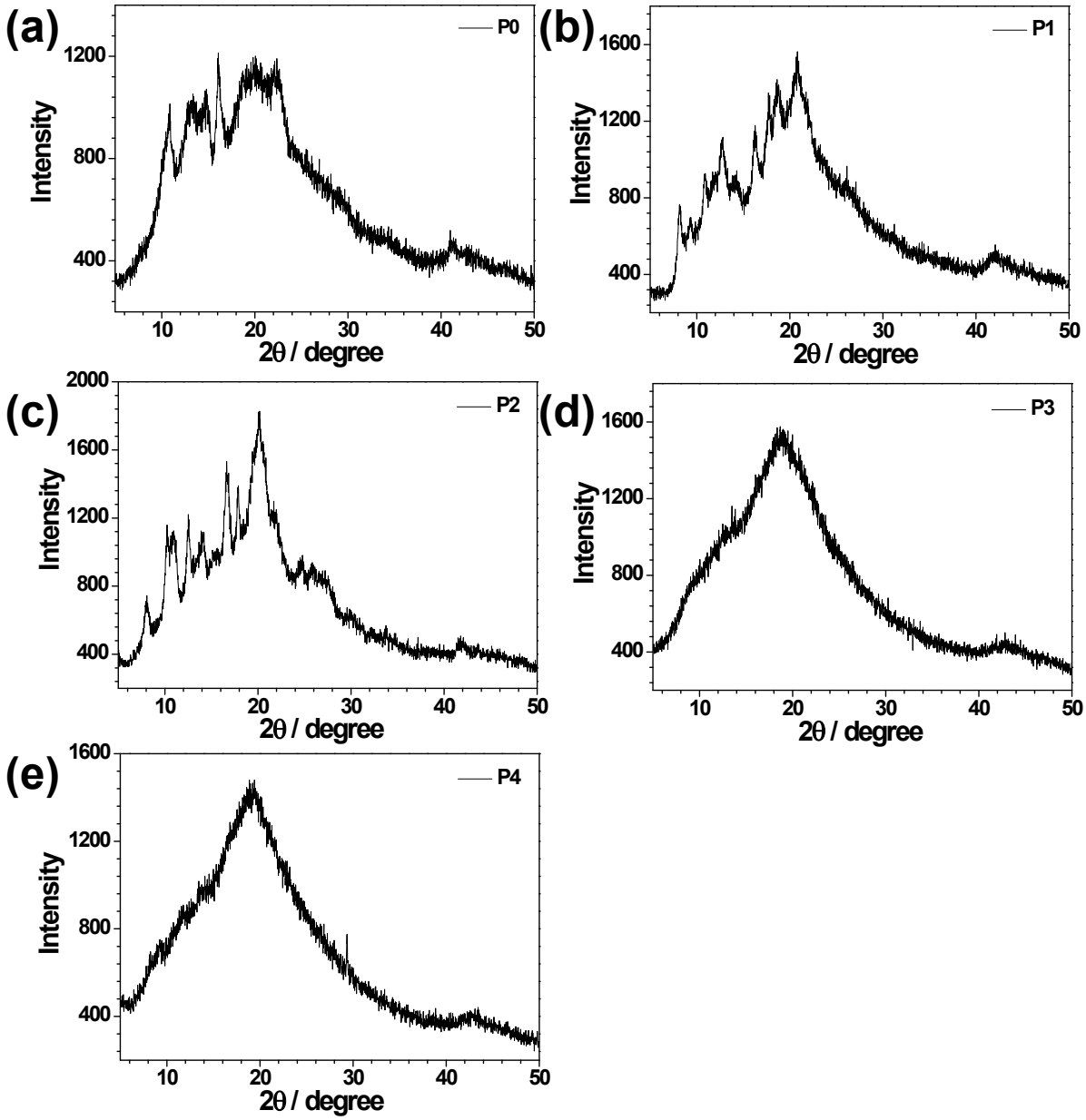

Figure S27. The Powder-XRD patterns of **P0–4**.

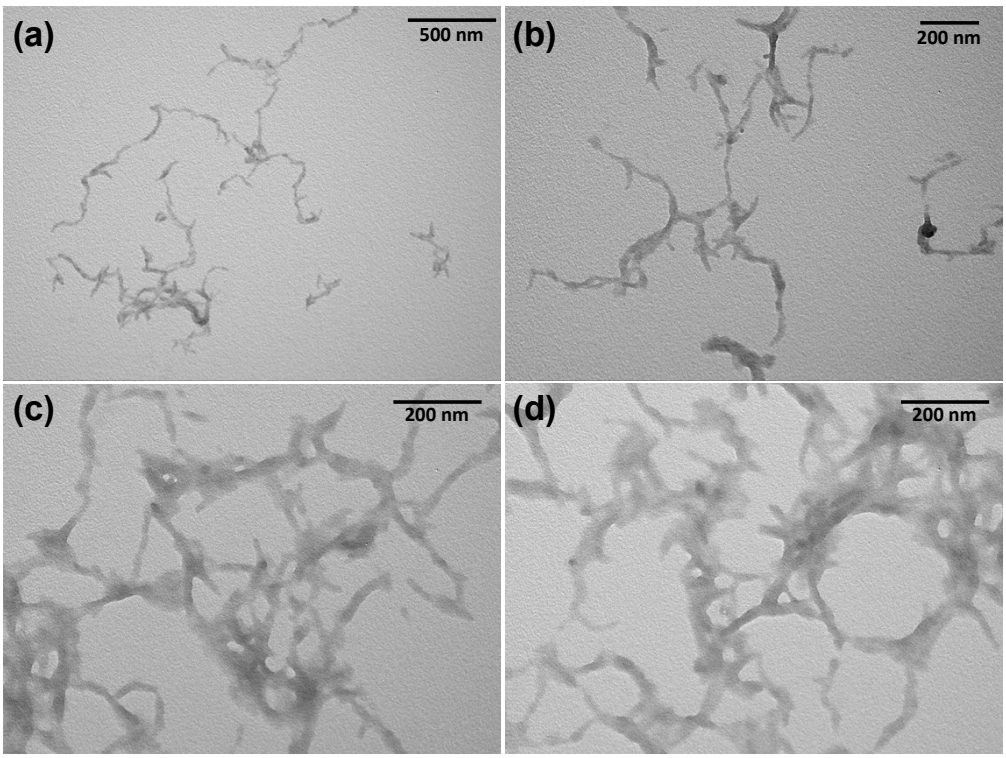

Figure S28. TEM images of the sample of **P1** prepared by spin-coating on a silicon substrate from acetonitrile diluted solution of the polymer and dried in vacuo.

SI3 Photophysical properties of ligands and coordination polymers

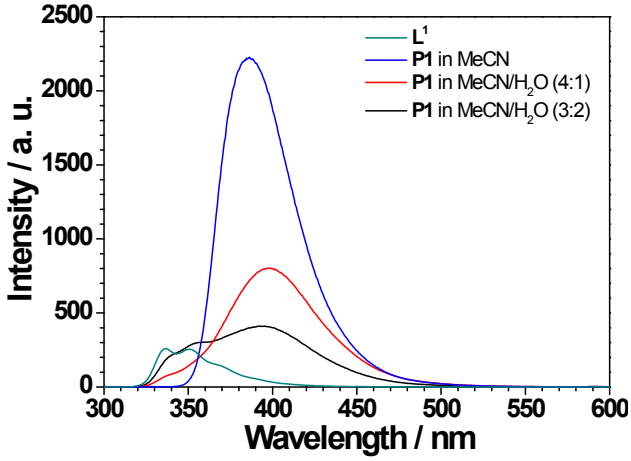

Figure S29. The fluorescence changes of **P1** after the increase of water content in the acetonitrile solution.

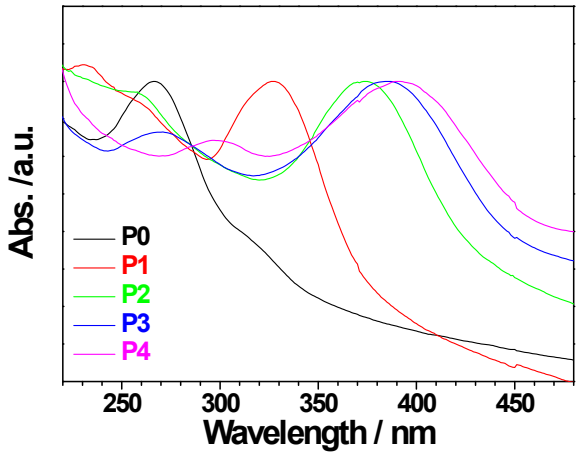

Figure S30. The normalized UV-vis spectra of the **P0–4** on a quartz glass substrate at room temperature.

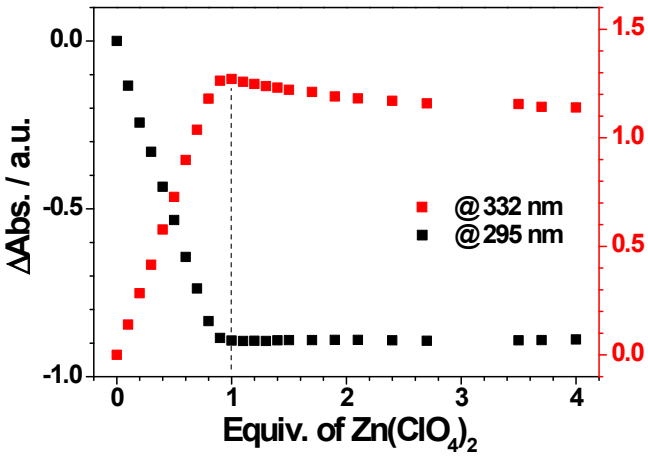

Figure S31. The normalized absorption at 295 nm and 332 nm as function of Zn^{2+} : $\mathbf{L^1}$ ratio.

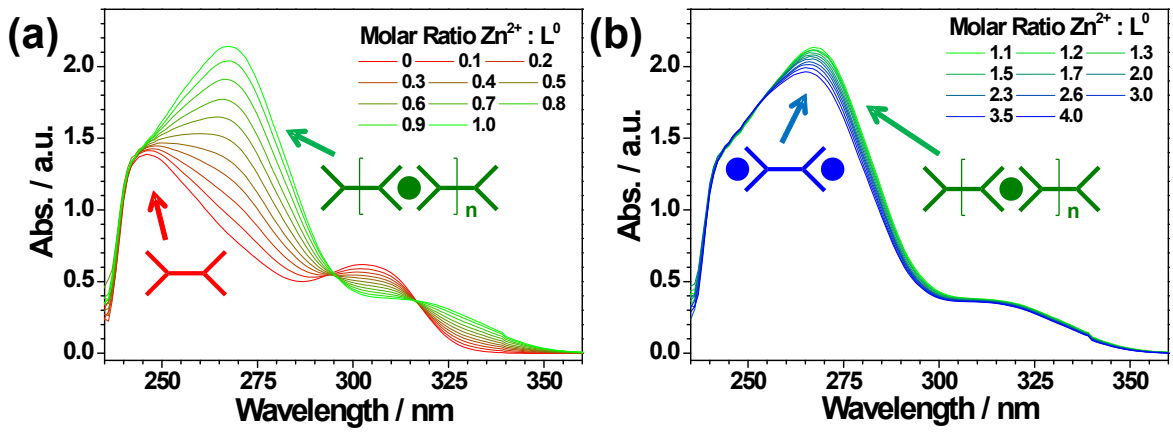

Figure S32. UV-vis spectra aquired upon titration of $\mathbf{L^0}$ in chloroform with $Zn(ClO_4)_2$. Shown are spectra at selected Zn^{2+} : $\mathbf{L^0}$ ratios ranging from 0 to 1 (a) and above 1 (b).

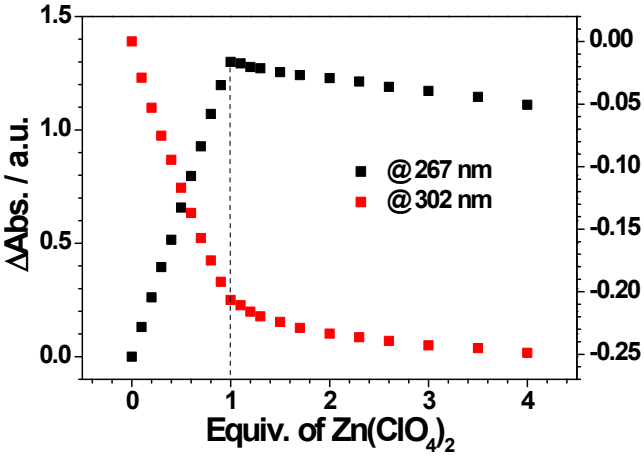

Figure S33. The normalized absorption at 267 nm and 302 nm as function of Zn^{2+} : $\mathbf{L^0}$ ratio.

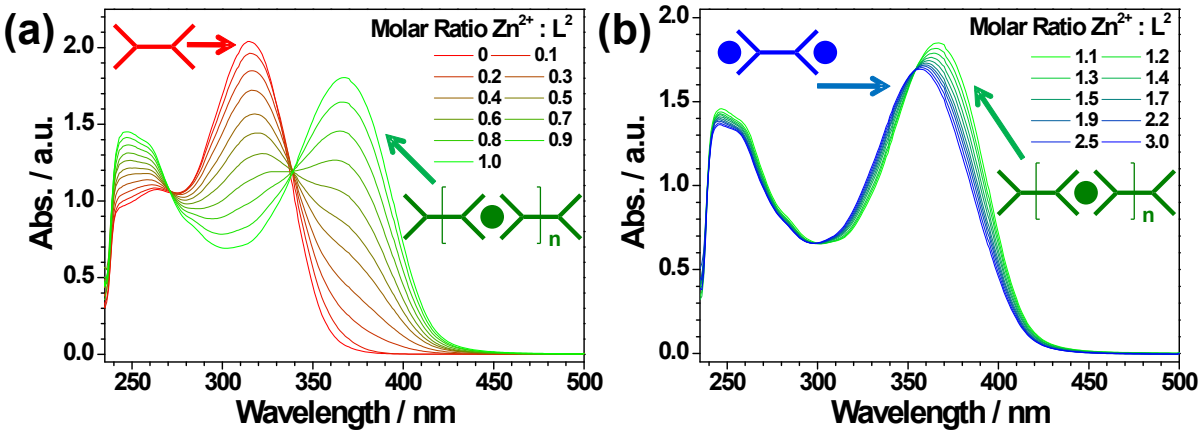

Figure S34. UV-vis spectra aquired upon titration of $\mathbf{L^2}$ in chloroform with $Zn(ClO_4)_2$. Shown are spectra at selected Zn^{2+} : $\mathbf{L^2}$ ratios ranging from 0 to 1 (a) and above 1 (b).

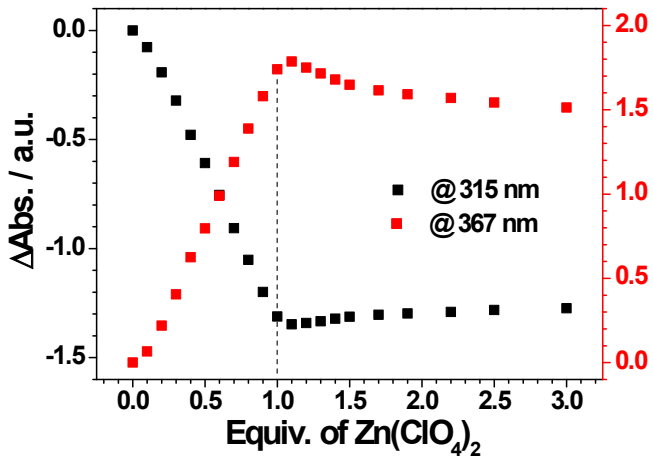

Figure S35. The normalized absorption at 315 nm and 367 nm as function of Zn^{2+} : $\mathbf{L^2}$ ratio.

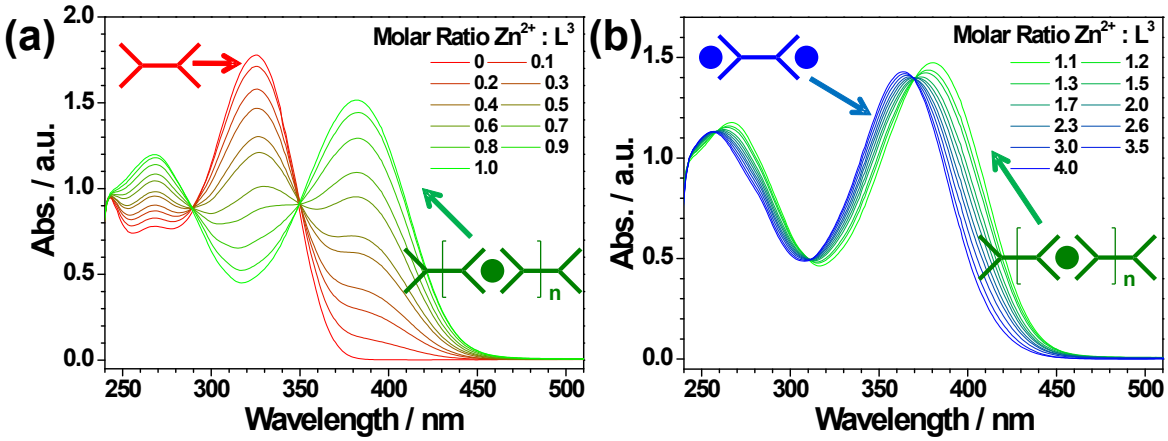

Figure S36. UV-vis spectra aquired upon titration of $\mathbf{L^3}$ in chloroform with $Zn(ClO_4)_2$. Shown are spectra at selected Zn^{2+} : $\mathbf{L^3}$ ratios ranging from 0 to 1 (a) and above 1 (b).

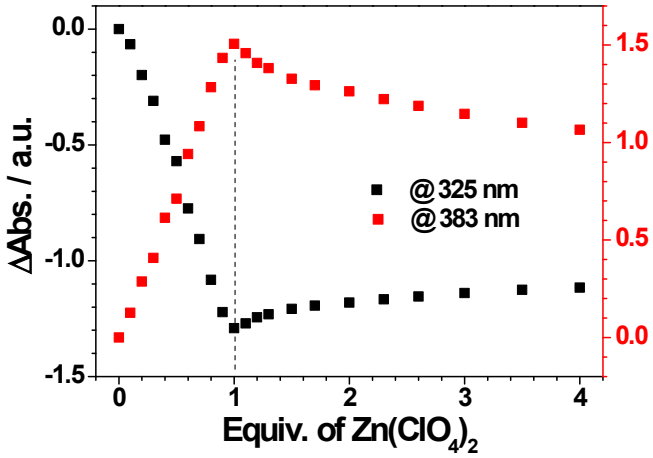

Figure S37. The normalized absorption at 325 nm and 383 nm as function of Zn^{2+} : $\mathbf{L^3}$ ratio.

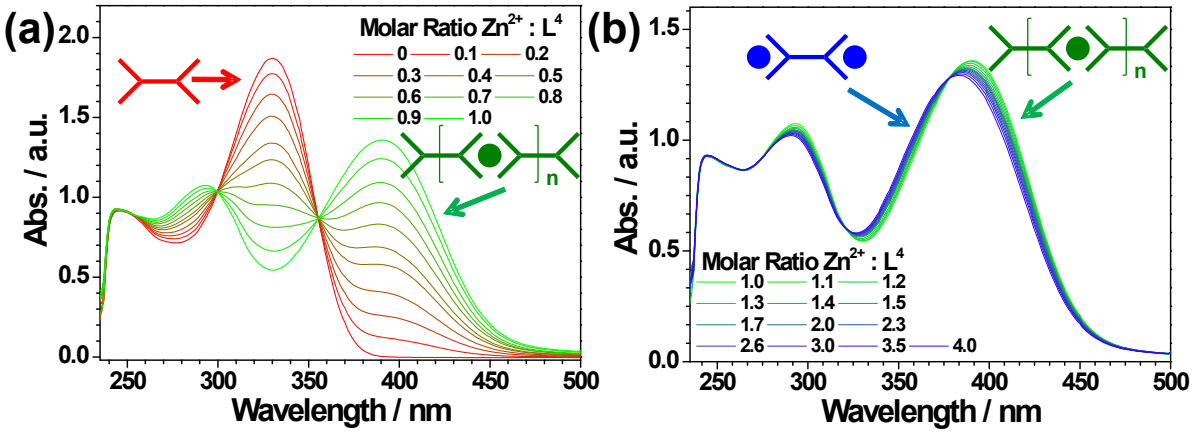

Figure S38. UV-vis spectra aquired upon titration of **L**^{4} in chloroform with $Zn(ClO_4)_2$. Shown are spectra at selected Zn^{2+} : **L**^{4} ratios ranging from 0 to 1 (a) and above 1 (b).

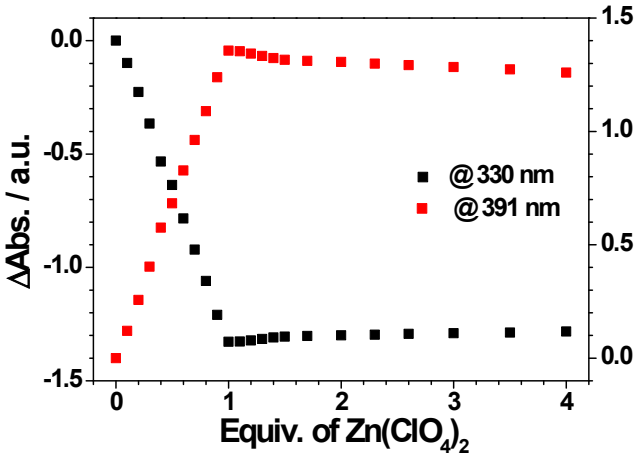

Figure S39. The normalized absorption at 330 nm and 391 nm as function of Zn^{2+} : **L**^{4} ratio.

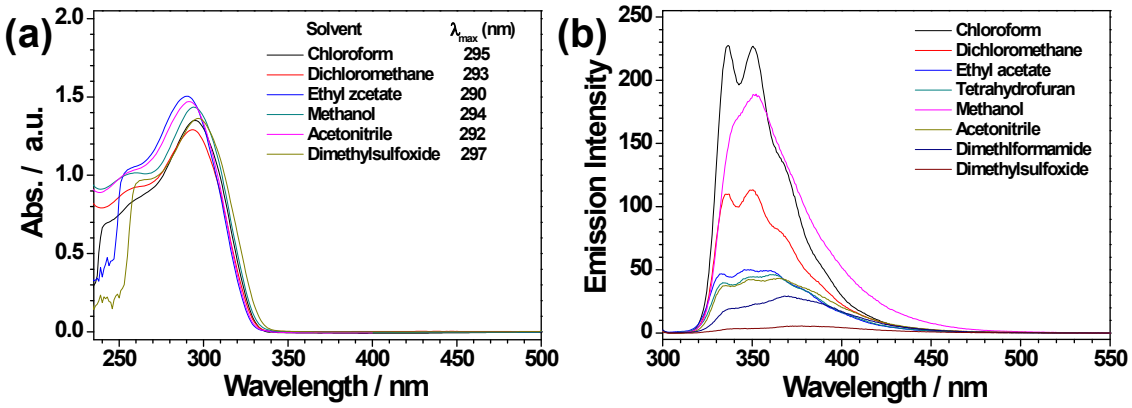

Figure S40. (a) UV-vis and (b) photoluminescence spectra of ligand **L**^{1} in different solvents.

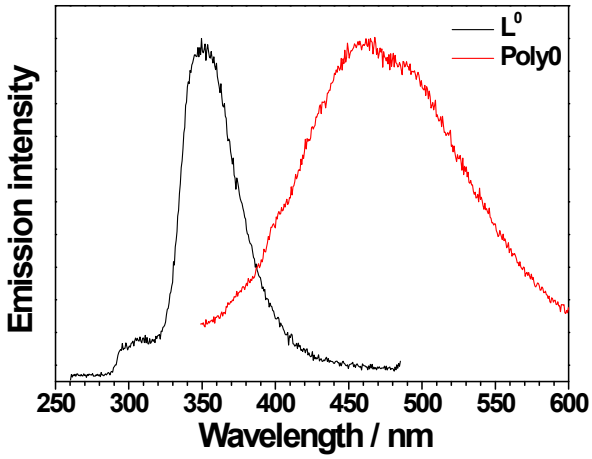

Figure S41. The normalized photoluminescence spectra of $\mathbf{L^0}$ in chloroform and **P0** in acetonitrile.

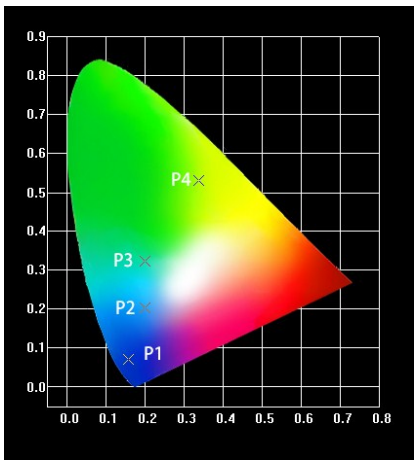

Figure S42. CIE chromaticity diagram showing the luminescence colors of **P1–4** (ClO_4^- forms) in acetonitrile solution, the luminescent colors of the **P1–4** were confirmed to be blue (x: 0.16; y: 0.07), cyan (x: 0.20; y: 0.20), light cyan (x: 0.20; y: 0.32), and yellow (x: 0.34; y: 0.53), respectively.

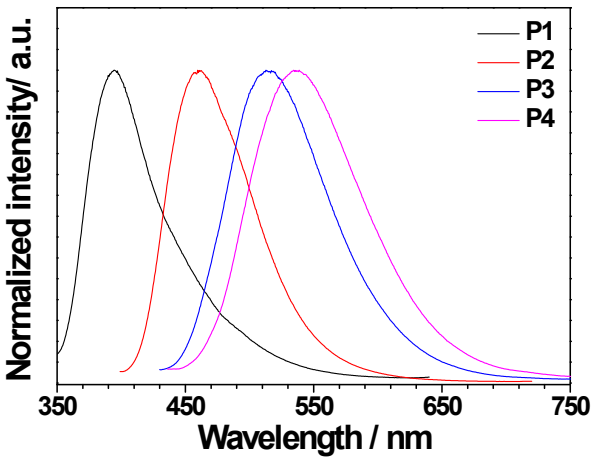

Figure S43. The normalized photoluminescence spectra of the **P1–4** on a quartz glass substrate at room temperature.

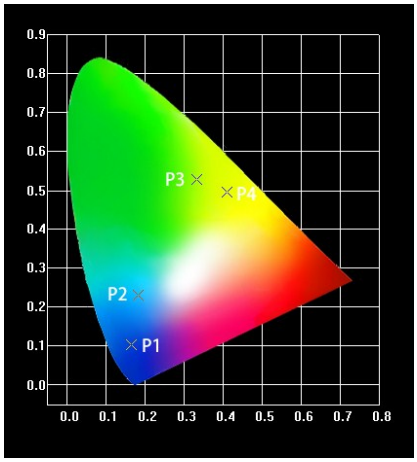

Figure S44. CIE chromaticity diagram showing the luminescence colors of **P1–4** ($CF_3SO_3^-$ forms) in film state, the luminescent colors of the **P1–4** were confirmed to be blue (x: 0.16; y: 0.10), cyan (x: 0.18; y: 0.23), yellow-green (x: 0.33; y: 0.53), and yellow (x: 0.41; y: 0.50), respectively.

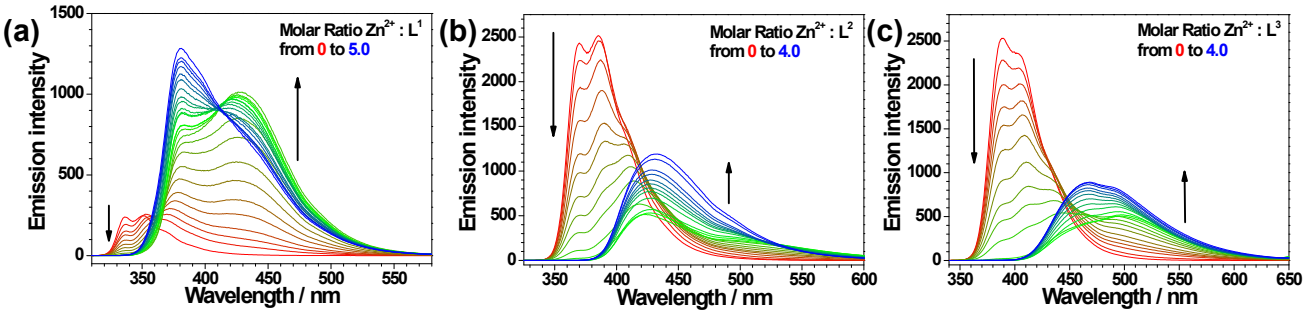

Figure S45. Fluorescent titration spectra of (a) $\mathbf{L^1}$, (b) $\mathbf{L^2}$, and (c) $\mathbf{L^3}$ (3×10^{-5} M) in chloroform with gradual addition of $Zn(ClO_4)_2$.

SI4 Dectection of PA

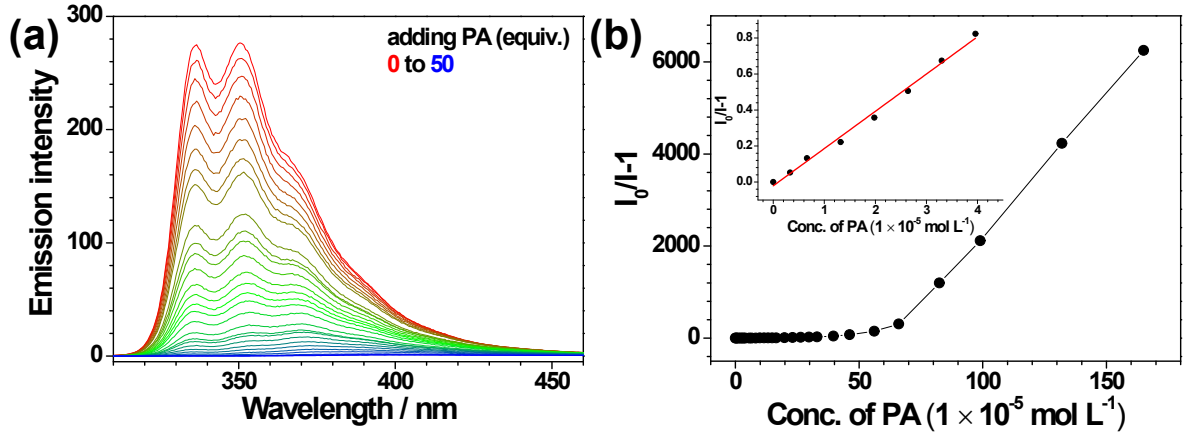

Figure S46. (a) Changes in fluorescence spectra of **L**[1] (3.3×10^{-5} mol L^{-1}) with the addition of PA in chloroform; (b) Stern-Volmer plot in response to PA. Inset: Linear Stern-Volmer plot obtained at lower concentration range of PA.

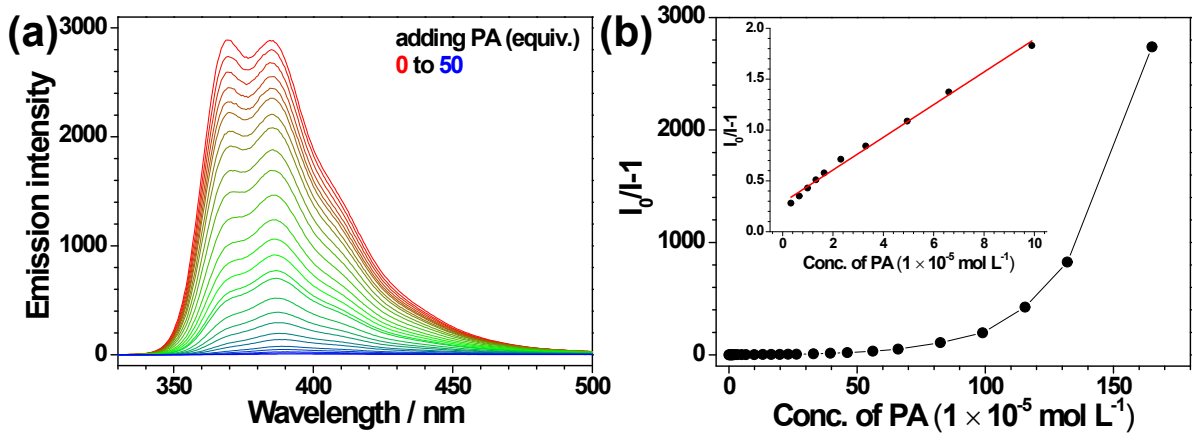

Figure S47. (a) Changes in fluorescence spectra of **L**[2] (3.3×10^{-5} mol L^{-1}) with the addition of PA in chloroform; (b) Stern-Volmer plot in response to PA. Inset: Linear Stern-Volmer plot obtained at lower concentration range of PA.

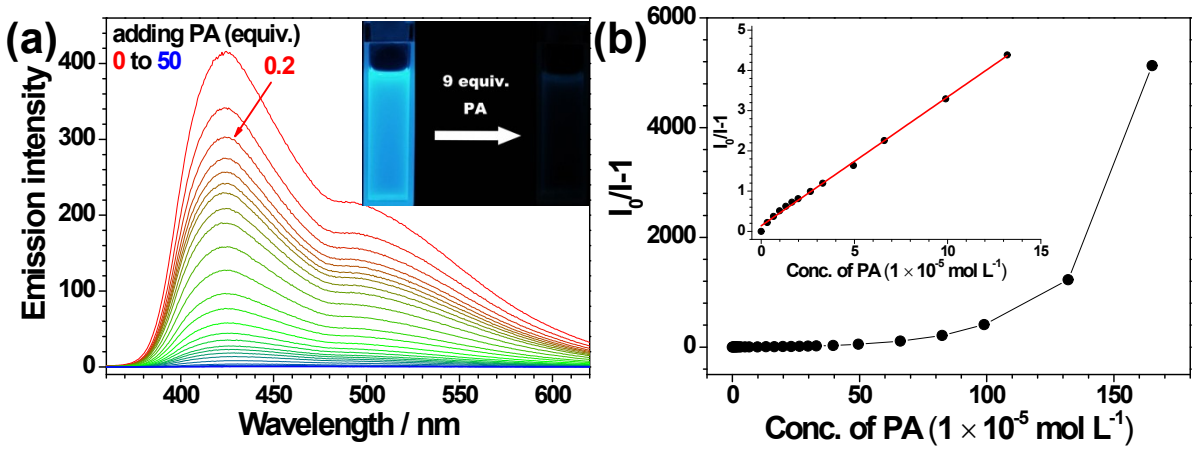

Figure S48. (a) Changes in fluorescence spectra of **P2** (3.3×10^{-5} mol L^{-1}) with the addition of PA in chloroform. Inset: change in the emission color after the addition of 9 equiv. of PA; (b) Stern-Volmer plot in response to PA. Inset: Linear Stern-Volmer plot obtained at lower concentration range of PA.

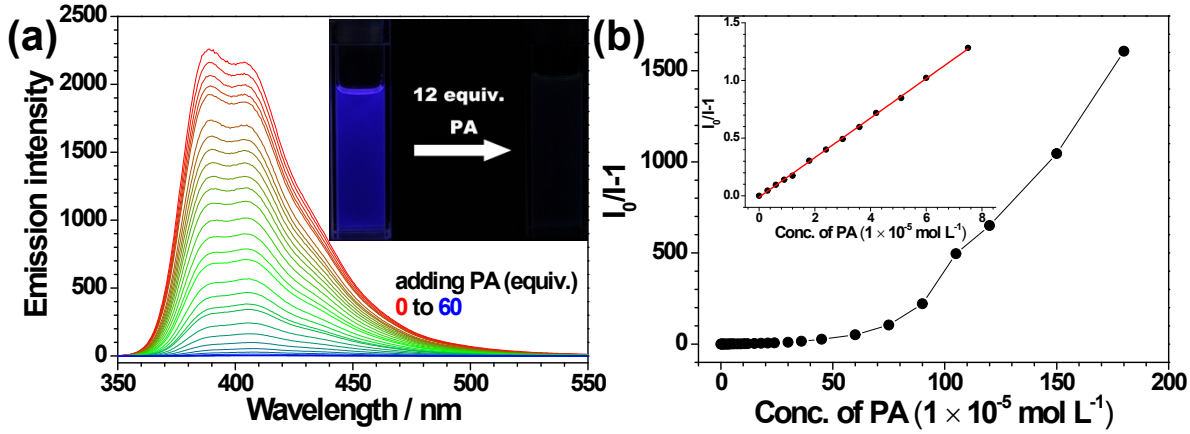

Figure S49. (a) Changes in fluorescence spectra of $\mathbf{L^3}$ (3×10^{-5} mol L^{-1}) with the addition of PA in chloroform; (b) Stern-Volmer plot in response to PA. Inset: Linear Stern-Volmer plot obtained at lower concentration range of PA.

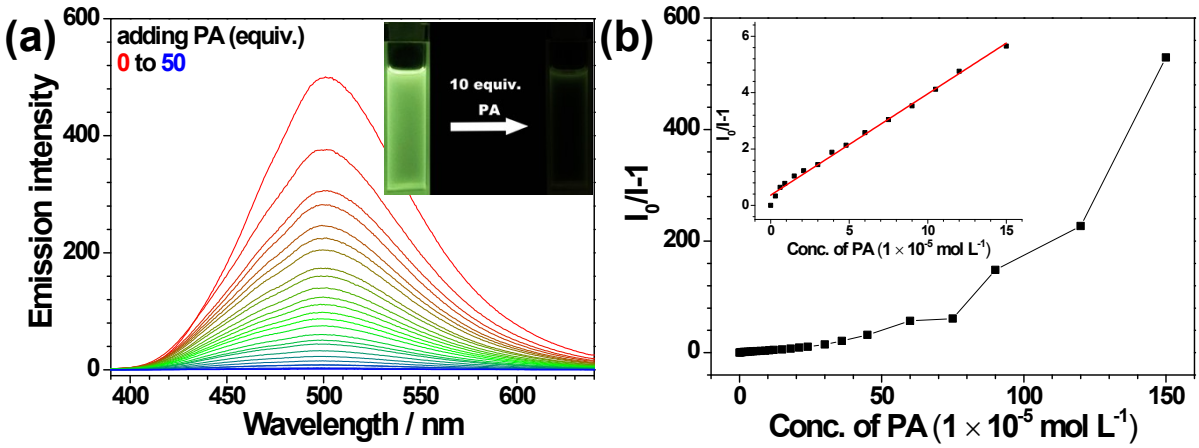

Figure S50. (a) Changes in fluorescence spectra of **P3** (3×10^{-5} mol L^{-1}) with the addition of PA in chloroform. Inset: change in the emission color after the addition of 10 equiv. of PA; (b) Stern-Volmer plot in response to PA. Inset: Linear Stern-Volmer plot obtained at lower concentration range of PA.

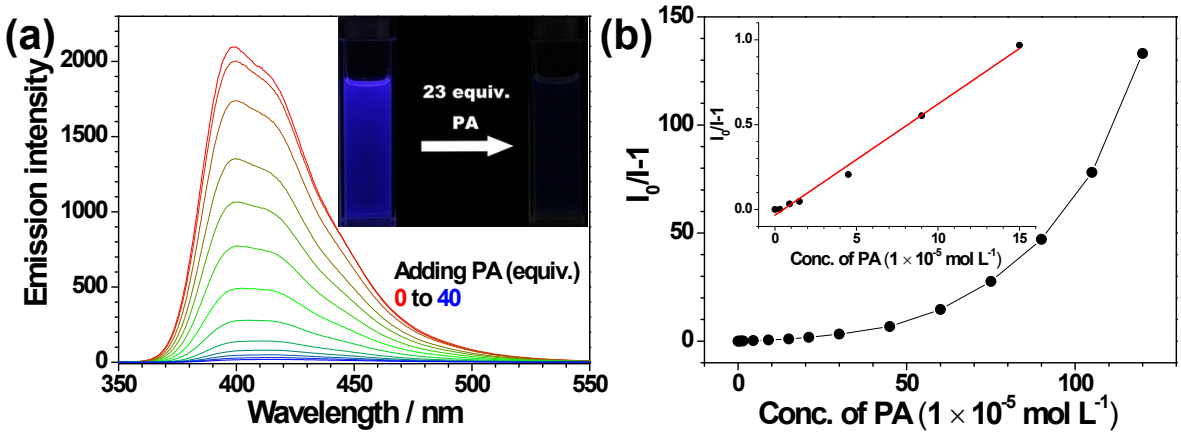

Figure S51. (a) Changes in fluorescence spectra of **L⁴** (3×10^{-5} mol L^{-1}) with the addition of PA in chloroform; (b) Stern-Volmer plot in response to PA. Inset: Linear Stern-Volmer plot obtained at lower concentration range of PA.

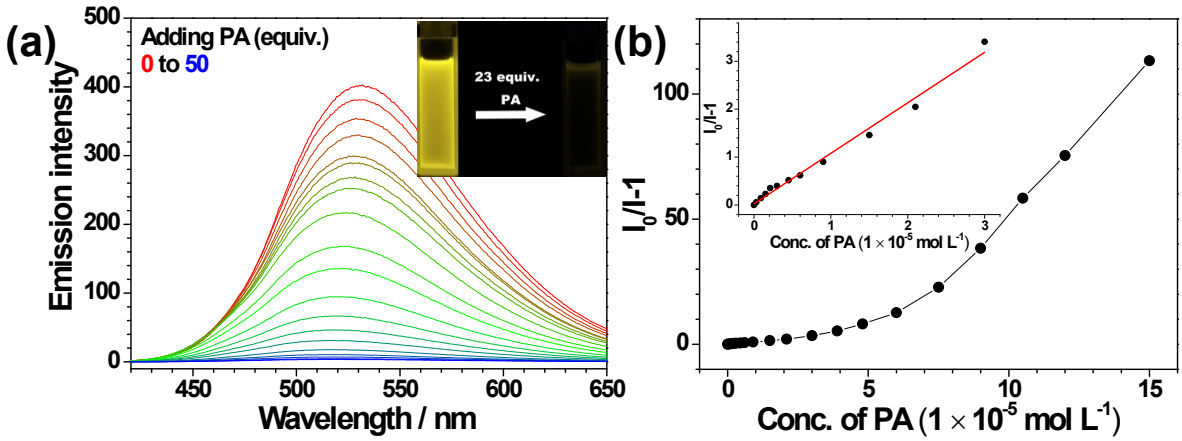

Figure S52. (a) Changes in fluorescence spectra of **P4** (3×10^{-5} mol L^{-1}) with the addition of PA in chloroform; (b) Stern-Volmer plot in response to PA. Inset: Linear Stern-Volmer plot obtained at lower concentration range of PA.

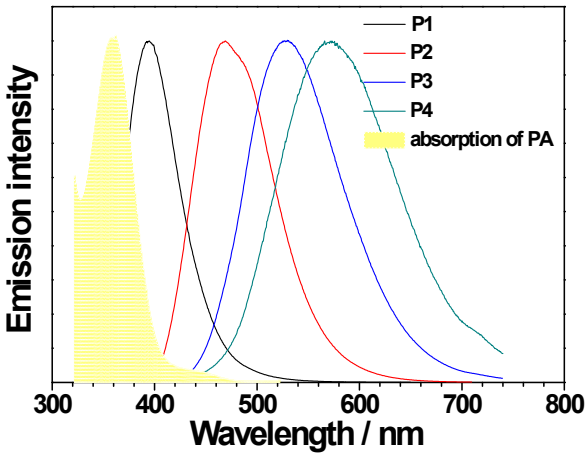

Figure S53. Spectral overlap of the absorption spectra of PA (yellow) with the emission spectra of **P1–4**.

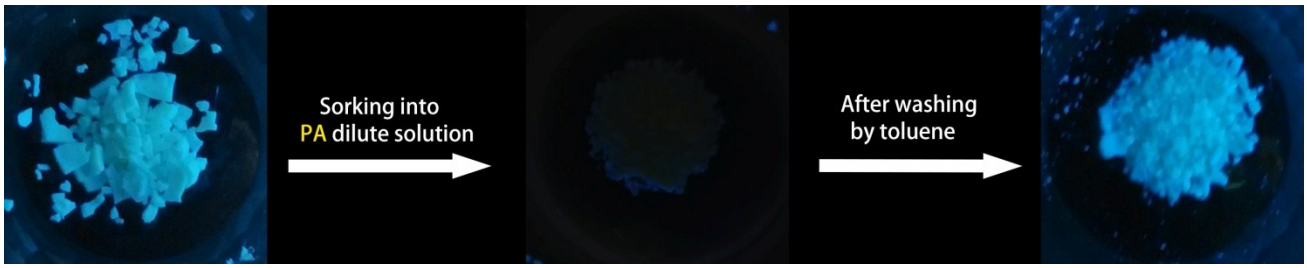

Figure S54. The sensing reversibility test of **P1** towards PA.

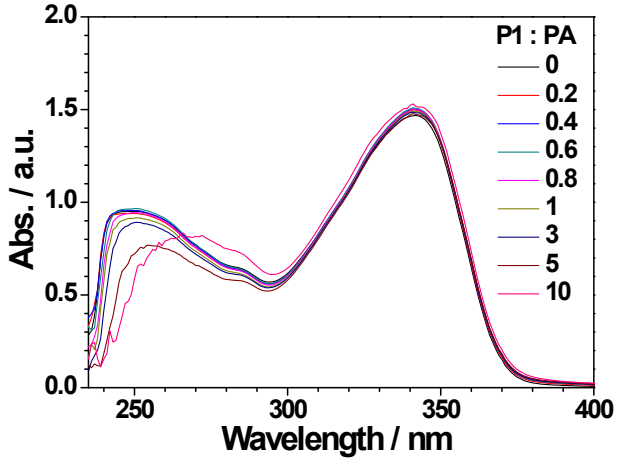

Figure S55. UV-vis spectra aquired upon titration of **P1** in chloroform with PA with **P1** : PA ratios ranging from 0 to 10.

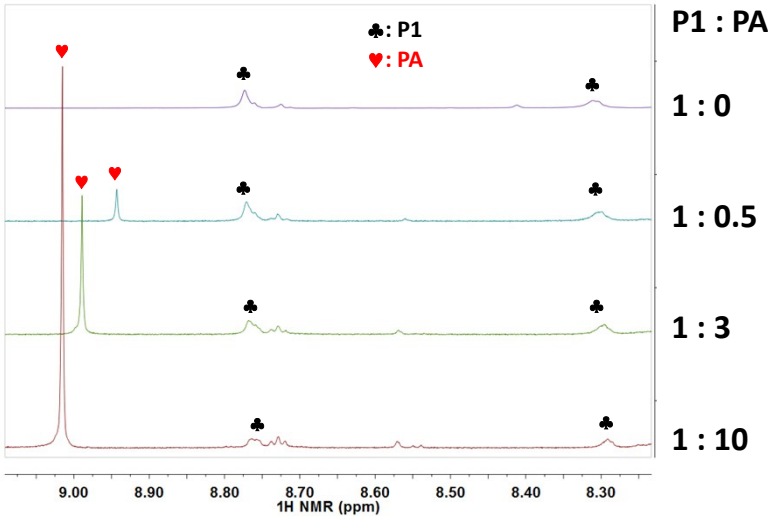

Figure S56. The ^{1}H NMR spectra of a mixture of **P1** and PA at different molar ratios in CD_3CN at 298 K (600 MHz).

Table S1. Amount of PA Resulting in 95% Fluorescence Quenching of Different Compounds, the Stern-Volmer constants and the detection limit values.

Entry	Compound	Amount (equiv.)	Stern-Volmer constant (K_{SV})	Detection Limit (DL) (ppb)
1	**L^1**	8	2.07×10^4	6660
2	**L^2**	17	1.61×10^4	3930
3	**L^3**	12	1.71×10^4	2400
4	**L^4**	23	6.55×10^3	5540
5	**P1**	1	5.51×10^5	46.7
6	**P2**	9	3.20×10^4	695
7	**P3**	10	3.60×10^4	1390
8	**P4**	23	1.05×10^4	1770

Table S2. Amount of Different NACs Resulting in 95% Fluorescence Quenching of Coordination Polymer **P1**.

Entries	NACs	Chemical structures	Amount (equiv.)
1	PA	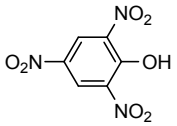	1
2	*p*-NP	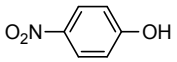	8
3	DMNP	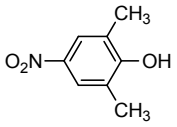	17
4	*o*-NP	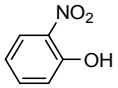	25
5	NBA	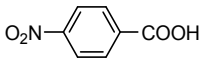	35
6	NBD	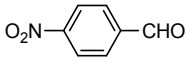	40
7	*m*-DNP	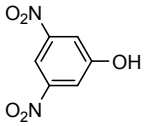	50
8	NB	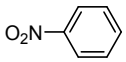	55
9	CDNB	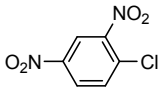	80
10	DNB	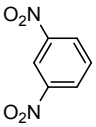	100

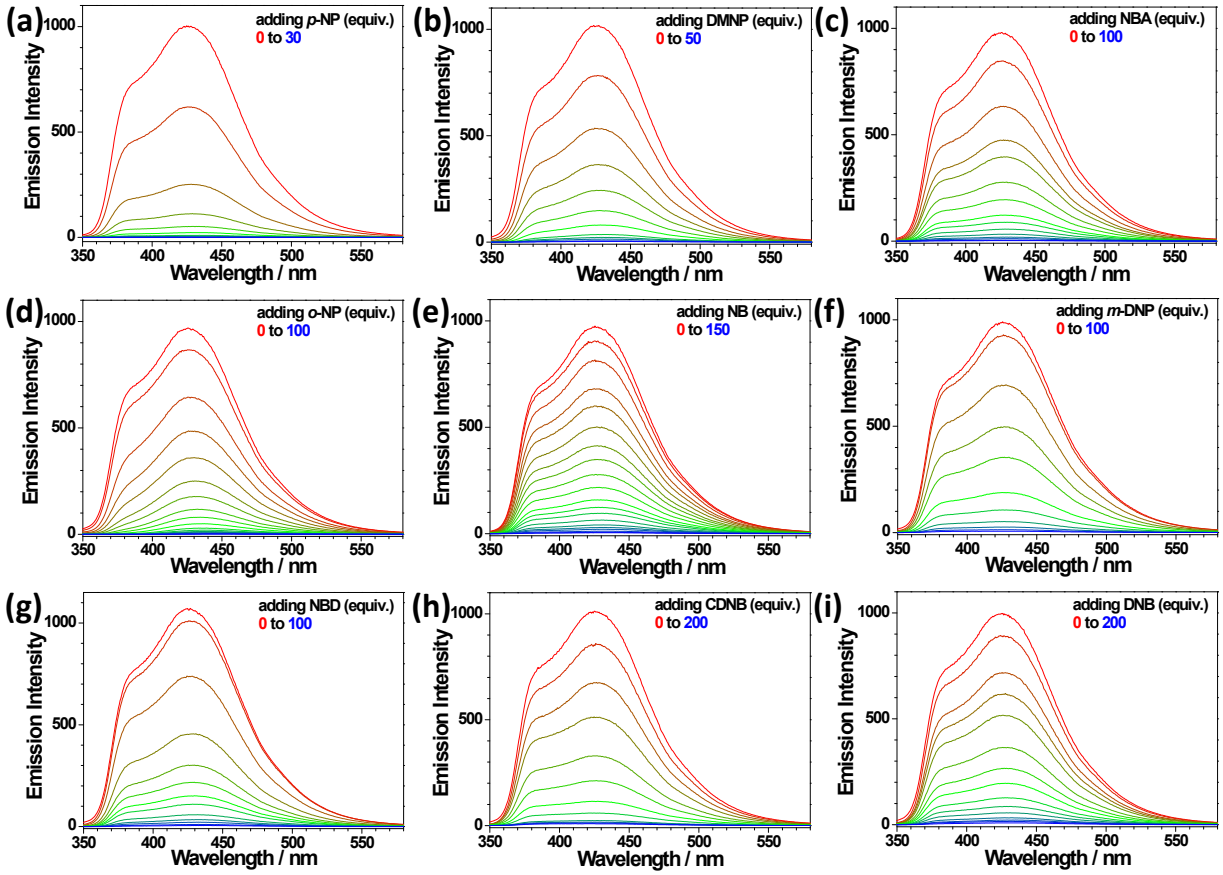

Figure S57. Changes in fluorescence spectra of P1 (3×10^{-5} mol L^{-1}) with the addition of different NACs in chloroform. (a) 4-nitrophenal (*p*-NP), (b) 2,6-dimethyl-4-nitrophenol (DMNP), (c) 4-nitrobenzoic acid (NBA), (d) 2-nitrophenol (*o*-NP), (e) nitrobenzene (NB), (f) 3,5-dinitrophenol (*m*-DNP), (g) 4-nitrobenzaldehyde (NBD), (h) 1-chloro-2,4-dinitrobenzene (CDNB), and (i) 1,3-dinitrobenzene (DNB).